This paper is published as part of a *PCCP* themed issue on characterisation of adsorbed species

Guest Editors: Petr Nachtigall and Carlos Otero Arean

Editorial

Themed Issue on characterisation of adsorbed species
Petr Nachtigall and Carlos Otero Arean, *Phys. Chem. Chem. Phys.*, 2010
DOI: 10.1039/c0cp90026e

Perspective

Hydroxyapatite as a key biomaterial: quantum-mechanical simulation of its surfaces in interaction with biomolecules
Marta Corno, Albert Rimola, Vera Bolis and Piero Ugliengo, *Phys. Chem. Chem. Phys.*, 2010
DOI: 10.1039/c002146f

Communications

Hydrogen induced CO activation on open Ru and Co surfaces
Sharan Shetty and Rutger A. van Santen, *Phys. Chem. Chem. Phys.*, 2010
DOI: 10.1039/b926731j

Large heterogeneity of Brønsted acid sites in ASA and USY zeolites: evidencing a third acidic component
Olivier Cairon, *Phys. Chem. Chem. Phys.*, 2010
DOI: 10.1039/c000991a

Papers

Simultaneous adsorption of benzene and dioxygen in CuHY zeolites as a precursor process to the aerobic oxidation of benzene to phenol
Shampa Santra, Hermann Stoll and Guntram Rauhut, *Phys. Chem. Chem. Phys.*, 2010
DOI: 10.1039/b921531j

Physisorption of aromatic organic contaminants at the surface of hydrophobic/hydrophilic silica geosorbents: a B3LYP-D modeling study
Albert Rimola, Bartolomeo Civalleri and Piero Ugliengo, *Phys. Chem. Chem. Phys.*, 2010
DOI: 10.1039/c000009d

Formation of O adatom pairs and charge transfer upon O_2 dissociation on reduced TiO_2(110)
Yingge Du, Nathaniel A. Deskins, Zhenrong Zhang, Zdenek Dohnalek, Michel Dupuis and Igor Lyubinetsky, *Phys. Chem. Chem. Phys.*, 2010
DOI: 10.1039/c000250j

Study of polycyclic aromatic hydrocarbons adsorbed on graphene using density functional theory with empirical dispersion correction
Olga V. Ershova, Timothy C. Lillestolen and Elena Bichoutskaia, *Phys. Chem. Chem. Phys.*, 2010
DOI: 10.1039/c000370k

DFT/CC investigation of physical adsorption on a graphite (0001) surface
Miroslav Rubeš, Jiří Kysilka, Petr Nachtigall and Ota Bludský, *Phys. Chem. Chem. Phys.*, 2010
DOI: 10.1039/c001155j

Monitoring the interaction of adsorbates on metal surfaces by surface site engineering: the case of ethoxy on Cu, Pd, Ag and Au regular and stepped surfaces
Juan Radilla, Mercé Boronat, Avelino Corma and Francesc Illas, *Phys. Chem. Chem. Phys.*, 2010
DOI: 10.1039/c000405g

Adsorption of oxygen on copper in Cu/HZSM5 zeolites
Augusta Bianca Ene, Matthias Bauer, Tanja Archipov and Emil Roduner, *Phys. Chem. Chem. Phys.*, 2010
DOI: 10.1039/c000750a

Elucidation of consistent enantioselectivity for a homologous series of chiral compounds in homochiral metal–organic frameworks
Xiaoying Bao, Linda J. Broadbelt and Randall Q. Snurr, *Phys. Chem. Chem. Phys.*, 2010
DOI: 10.1039/c000809e

A DFT study of PtAu bimetallic clusters adsorbed on MgO/Ag(100) ultrathin films
Sabrina Sicolo and Gianfranco Pacchioni, *Phys. Chem. Chem. Phys.*, 2010
DOI: 10.1039/c000841a

CO as an IR probe molecule for characterization of copper ions in a basolite C300 MOF sample
Nikola Drenchev, Elena Ivanova, Mihail Mihaylov and Konstantin Hadjiivanov, *Phys. Chem. Chem. Phys.*, 2010
DOI: 10.1039/c000949k

Existence of dual species composed of Cu^+ in CuMFI being bridged by C_2H_2
Atsushi Itadani, Takashi Yumura, Takahiro Ohkubo, Hisayoshi Kobayashi and Yasushige Kuroda, *Phys. Chem. Chem. Phys.*, 2010
DOI: 10.1039/c000967a

Benchmark calculations of water–acene interaction energies: Extrapolation to the water–graphene limit and assessment of dispersion–corrected DFT methods
Glen R. Jenness, Ozan Karalti and Kenneth D. Jordan,

Phys. Chem. Chem. Phys., 2010
DOI: 10.1039/c000988a

Adsorption of light hydrocarbons in the flexible MIL-53(Cr) and rigid MIL-47(V) metal–organic frameworks: a combination of molecular simulations and microcalorimetry/gravimetry measurements
N. Rosenbach Jr, A. Ghoufi, I. Déroche, P. L. Llewellyn, T. Devic, S. Bourrelly, C. Serre, G. Férey and G. Maurin, *Phys. Chem. Chem. Phys.*, 2010
DOI: 10.1039/c001173h

Role of dispersive interactions in the CO adsorption on MgO(001): periodic B3LYP calculations augmented with an empirical dispersion term
Bartolomeo Civalleri, Lorenzo Maschio, Piero Ugliengo and Claudio M. Zicovich-Wilson, *Phys. Chem. Chem. Phys.*, 2010
DOI: 10.1039/c001192d

Nature and role of surface carbonates and bicarbonates in CO oxidation over RuO_2
Hangyao Wang and William F. Schneider, *Phys. Chem. Chem. Phys.*, 2010
DOI: 10.1039/c001683g

Experimental and theoretical determination of adsorption heats of CO_2 over alkali metal exchanged ferrierites with different Si/Al ratio
Arnošt Zukal, Angeles Pulido, Barbara Gil, Petr Nachtigall, Ota Bludský, Miroslav Rubeš and Jiří Čejka, *Phys. Chem. Chem. Phys.*, 2010
DOI: 10.1039/c001950j

Six-dimensional dynamics study of reactive and non reactive scattering of H_2 from Cu(111) using a chemically accurate potential energy surface
C. Díaz, R. A. Olsen, D. J. Auerbach and G. J. Kroes, *Phys. Chem. Chem. Phys.*, 2010
DOI: 10.1039/c001956a

Azobenzene *versus* 3,3′,5,5′-tetra-*tert*-butyl-azobenzene (TBA) at Au(111): characterizing the role of spacer groups
Erik R. McNellis, Christopher Bronner, Jörg Meyer, Martin Weinelt, Petra Tegeder and Karsten Reuter, *Phys. Chem. Chem. Phys.*, 2010
DOI: 10.1039/c001978j

FTIR spectroscopy and thermodynamics of CO and H_2 adsorbed on γ-, δ- and α-Al_2O_3
Evgeniy N. Gribov, Olena Zavorotynska, Giovanni Agostini, Jenny G. Vitillo, Gabriele Ricchiardi, Giuseppe Spoto and Adriano Zecchina, *Phys. Chem. Chem. Phys.*, 2010
DOI: 10.1039/c002031c

A highly ordered, aromatic bidentate self-assembled monolayer on Au(111): a combined experimental and theoretical study
Xia Stammer, Katrin Tonigold, Asif Bashir, Daniel Käfer, Osama Shekhah, Christian Hülsbusch, Martin Kind, Axel Groß and Christof Wöll, *Phys. Chem. Chem. Phys.*, 2010
DOI: 10.1039/c002215m

Modelling active sites for the Beckmann rearrangement reaction in boron-containing zeolites and their interaction with probe molecules
Inés Lezcano-González, Alejandro Vidal-Moya, Mercedes Boronat, Teresa Blasco and Avelino Corma, *Phys. Chem. Chem. Phys.*, 2010
DOI: 10.1039/c002427a

A FTIR search for linkage isomerism of CN^- ions adsorbed on oxides and zeolites
A. A. Tsyganenko, A. M. Chizhik and A. I. Chizhik, *Phys. Chem. Chem. Phys.*, 2010
DOI: 10.1039/c003942j

PCCP

Physical Chemistry Chemical Physics

www.rsc.org/pccp

Volume 12 | Number 24 | 28 June 2010 | Pages 6293–6536

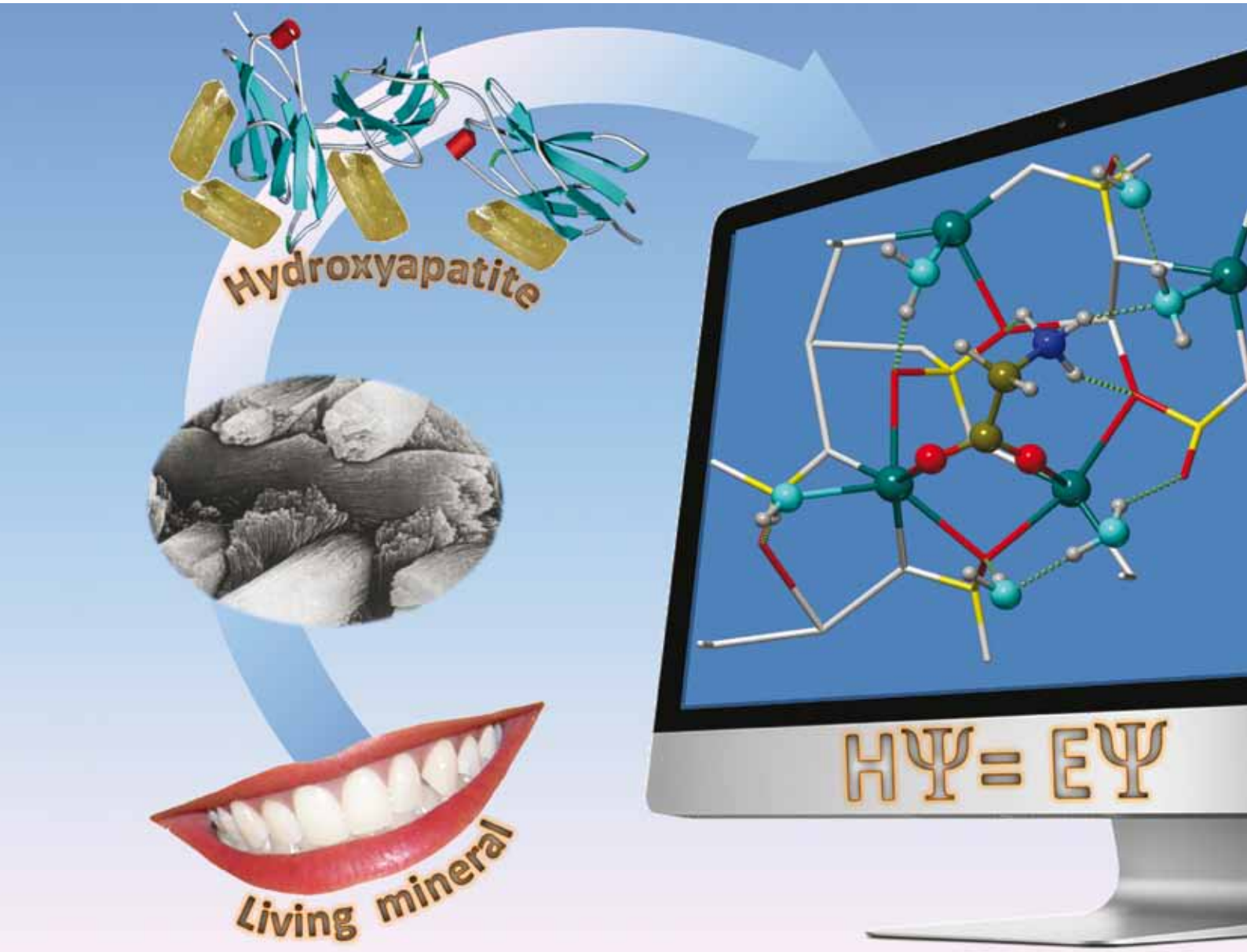

Themed Issue: Characterization of adsorbed species

ISSN 1463-9076

1463-9076(2010)12:24;1-#

Hydroxyapatite as a key biomaterial: quantum-mechanical simulation of its surfaces in interaction with biomolecules

Marta Corno,[a] Albert Rimola,[a] Vera Bolis[b] and Piero Ugliengo*[a]

Received 1st February 2010, Accepted 15th April 2010
First published as an Advance Article on the web 18th May 2010
DOI: 10.1039/c002146f

Hydroxyapatite is the mineral component of human bones and teeth enamel and is used as synthetic biomaterial. It also grows outside bioglasses as a response of their incorporation in body fluids. The focus is then on understanding the microscopic steps occurring at its surfaces as this allows researchers to understand the key features of biomolecular adhesion. This perspective article deals with *in silico* simulations of these processes by quantum-mechanical methods based on density functional theory using the hybrid B3LYP functional and Gaussian basis functions.

Introduction

In the last decades highly sophisticated experimental techniques[1–4] have been fruitfully coupled, in an increasing number of cases, with modelling techniques derived from rigorous quantum-mechanical methods to model the surface of materials. In this way, the microscopic features of metallic materials, as well as of semiconductors and insulators,[5–7] involved in a huge variety of chemical processess relevant to the development of modern society,[8] have been thoroughly understood. As an example to illustrate this kind of successful physico-chemical approach, we can mention the case of the Haber-Bosch NH_3-synthesis reaction which was understood at molecular detail thanks to the concentrated effort of Gerhard Ertl's group. Indeed, since the early seventies, this team has set up an impressive arsenal of experimental techniques run under highly controlled conditions to fully characterize the microscopic steps of the reaction.[9] In parallel, quantum-mechanical simulation based on density functional theory has recently demonstrated its increasing power in characterizing the potential energy surface of all Haber-Bosch reaction steps, as catalyzed by Ru nanoparticles, in fairly good agreement with experiments.[10] In this respect, the joint use of the whole set of surface science experimental techniques, together with the best first principle calculations available today, contributed to defining a successful "surface science model for catalysis" as it was defined by Castner and Ratner in their fundamental review.[11] From an experimental point of view, however, there are several limits to the applications of the typical surface science techniques.[4] Ultra high vacuum (UHV) conditions, which are essential to many of the surface science techniques and which permit clean surfaces to be prepared and maintained, are almost invariably adopted. Low-energy electron diffraction (LEED) or scanning tunnelling microscopy (STM), for instance, are in general able to give important details of the adsorbent/adsorbate interface

[a] *Dipartimento di Chimica IFM, NIS Centre of Excellence and INSTM (Materials Science and Technology) National Consortium, UdR Torino, Via P. Giuria 7, Torino, Italy. E-mail: piero.ugliengo@unito.it; Fax: +390112364596; Tel: +390116704596*
[b] *Dipartimento DiSCAFF, Università del Piemonte Orientale "A. Avogadro", Novara and INSTM (Materials Science and Technology) National Consortium, UdR Piemonte Orientale, Italy*

Marta Corno

Marta Corno received her Laurea degree and PhD in Chemical Sciences at the University of Turin in 2004 and 2007, respectively, in the research group of Prof. Piero Ugliengo. At present she is a postdoctoral researcher in this group at the Department of Chemistry IFM in Turin. Her research interests concern the study of biomaterials, such as hydroxyapatite and bioactive glasses by means of high-level periodic quantum-mechanical calculations. Recently, she has started working on ab initio calculations on hydrogen storage materials, such as light metal hydrides.

Albert Rimola

Albert Rimola received his BS in Chemistry from the Autonomous University of Barcelona (UAB), where he completed in 2007 his PhD in Theoretical and Computational Chemistry under the supervision of Prof. Mariona Sodupe. Then he continued his studies as a post-doctoral researcher at the University of Torino for two years with Prof. Piero Ugliengo, focusing his research on modeling the interaction and reactivity of biomolecules with inorganic biomaterials for application in nanobiotechnology and prebiotic chemistry. In 2010 he returned to UAB to work on ab initio molecular dynamics of hydrated inorganic materials.

structure when the adsorbent is a well defined (non-defective) material and the adsorptive is a rather simple (few atoms) highly symmetric molecule. Despite these limits, just to mention a few rather complex examples, very interesting results have been obtained in describing the restructurization of the Cu(001) surface induced by Li deposition,[12] as observed by STM, or in clarifying the CO poisoning of H_2/D_2 exchange catalyzed by the Pt(111) surface,[3] or in characterizing the complex surface unit cells of ultrathin alumina film on NiAl(110).[13]

Along the same line, the joint use of experimental and theoretical approach has become essential in characterizing the surface features and reactivity also of 'non ideal' systems of catalytic interest, as witnessed by the rich literature in the field.[14–18] It is customary to believe the surface science approach as limited to probing the features of ideal surfaces in ideal conditions, while chemical processes at "real" defective surfaces are often occurring at high pressure or even in wet conditions. This is particularly true when surface science encounters an increasingly important class of materials which are employed in biomedical fields, such as the so-called 'biomaterials' that replace or improve lost or impaired vital body functions in humans, as well as 'biosensors' for biomedical diagnostics.[19] According to a consensus definition, a solid biomaterial necessarily interfaces with a biological tissue and/or physiological fluid.[20] In particular, a bioactive material implanted in the body is expected to elicit a specific biological response at the implant-tissue interface (*biological fixation*), which occurs through molecular events depending on solid composition, structure and on surface features and reactivity.[21]

It would be in principle feasible to directly extend the methodological approach behind the "surface science model for catalysis" towards a "surface science model for biology" in order to improve the understanding of the microscopic features of the biomaterial/biological system interface.[11,22,23] Unfortunately, this goal is still far from being achievable straightforwardly, not only because a living organism is intrinsically complex, but also because the implant/tissue interface is very large (~100–150 μm) with respect to the nanometric scale typical of molecular events occurring at the solid surface. Let us consider, for instance, a living cell interacting with a protein-covered biomaterial surface. Even reducing the system dramatically, by just focusing on the biomaterial surface interacting with the simplest among proteins, this is hardly characterized in structural details. However, a deep understanding of the fundamental molecular processes which take place at the solid biomaterial/biological system interface stems from the comprehension of the surface structure of the material and from the ability to design appropriate model systems mimicking the molecular components of a living cell.[19,23] An example of what can be achieved with state-of-art technology is the recent work by van de Keere *et al.*[24] on the interaction of human fibrinogen protein, whose structure is known at 2.9 Å resolution,[25] with Ti surfaces. The maximum level of structural detail is high enough (~10 nm) to distinguish the three protein domains but far from the detail needed to distinguish single protein atoms in contact with the surface. As a further complication, all processes at the biomaterial interface occur in the complexity of the body fluids. Despite these difficulties, the reductionist approach, in which simplified parts of a too complex system are studied independently and which has already been successfully adopted in catalysis studies, is very effective and, at the moment, the only feasible method of biological surface science studies.[23]

Among the huge variety of biomaterials (either metallic, polymeric or inorganic in nature) employed in biomedical applications, in the following we have chosen to focus mainly on hydroxyapatite (HA), a calcium phosphate mineral belonging to the crystal family of calcium apatites (HA, $[Ca_{10}(PO_4)_6X_2]$, with $X = OH^-$, Cl^-, F^- or Br^-). Hydroxyapatite is indeed the mineral component of human bones as well as of teeth enamel,[26] and its use as synthetic biomaterial is of obvious interest.[27] Recently, a large number

Vera Bolis

Vera Bolis (Laurea degree in Chemistry—University of Torino) is associate professor of inorganic chemistry at the University of Eastern Piedmont «A. Avogadro». She studies the surface properties of nano-sized inorganic materials especially with reference to their catalytic and/or biological activity, by means of adsorption microcalorimetry combined with spectroscopic techniques, modelling and electron microscopy. In recent years she has moved her research interests from heterogeneous catalysis towards the interaction of inorganic materials with living-matter components in order to identify the physico-chemical properties responsible for such interaction. She is co-author of ca. 100 scientific publications.

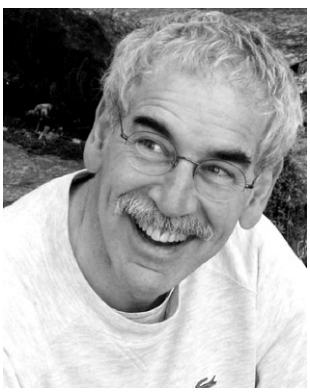

Piero Ugliengo

Piero Ugliengo received his Laurea degree in chemistry from the University of Torino where he is associate professor of physical chemistry working at the Department of Chemistry IFM. His main scientific interests are on ab initio modeling of hydrogen-bond interactions in solids and at their surfaces with focus on silica and zeolites. Recent projects are on modeling the role of minerals in pre-biotic chemistry and the adsorption process at the surface of inorganic biomaterials. He is co-author of about 130 papers.

of research papers have been published, dealing with the role and features of HA as a biomaterial,[28,29] investigated by means of both experimental[30–35] and theoretical[36–47] approaches. Only a few, however, have elucidated the structural details of the HA surface.

The ability of apatite-like materials to allow cells for a favorable adhesion and subsequent proliferation was also *put in evidence* by the *biological fixation* properties of bioactive glasses, *i.e.* the quaternary SiO_2–Na_2O–CaO–P_2O_5 mixed oxides prepared in the early 1970s by Hench and co-workers.[48–52] Such kind of glasses, which have been employed since then in restorative and regenerative medical applications, allow a layer of crystalline hydroxyl–carbonate apatite (HCA) to grow at their surface so ensuring bioactivity.[53] Indeed, in a pioneering work[50] Hench proposed that the formation of a strong and stable chemical bond between the 45S5 Bioglass® and rats' femurs is allowed by a sequence of chemical transformations occurring at the implanted material/living body interface, which leads to the formation of a HCA interface layer. This layer then interacts with and incorporates biomolecules such as collagen, whereas further cellular steps lead to a strong biological/chemical bond between the glass and human hard (bone) and, in some cases, soft (muscles) tissues.

In several experimental studies a variety of samples of either HA materials as such or after soaking in SBF (simulated body fluids, as suggested by Kokubo[54] as a test for bioactivity) have been investigated by means of different techniques, such as X-ray diffraction,[55] IR and Raman spectrometries,[56–58] microcalorimetry,[59,60] NMR[61] and many others. Furthermore, also several computational studies have been conducted either with molecular mechanics or by means of electronic structure methods,[36–38,40,62–64] in order to enlighten the HA materials (stoichiometric and non-stoichiometric) features, so contributing to the interpretation of the experimental results. It is also worth recalling that pure HA does not generally occur in biological systems,[22] but is most often present as the Ca-deficient and carbonate-containing apatite analogue. The effect of such substitutions (throughout the crystal or limited to the surface region) can be crucial in determining both bulk and surface chemistry properties of the biomaterial.

The focus of the present perspective is to illustrate the role of the quantum-mechanical simulation within the DFT realm to model both the bare HA surfaces and their interactions with molecules. Water and amino acids have been chosen as 'probe' molecules, the former to mimic the aqueous environment in which the biomaterial is employed, the latter as the simplest building block suitable for representing the more complex biomolecules constituting the organic part of the bone (collagen) or the cell membrane. It is not the purpose of this article to review the vast literature on this field: rather we will focus on the work having been developed in our own laboratory for a few years, which has the added value of being carried out using the same methodology from the very beginning. In essence, all calculations, irrespective of being for bulk or surfaces, have been carried *ab initio* within periodic boundary conditions as coded in the program CRYSTAL,[65] whose details will be given in the next section. It is our hope that this coherent approach, ensuring the constancy of systematic errors across all studied systems, would result in a robust modellistic framework to understand the hydroxyapatite structural features and its rich (bio)chemical behaviour.

Whereas comparison with available experimental data has always been addressed using literature results, for the case of water adsorption the computational results have been compared with the experimental data obtained within our own laboratory so that a more through discussion will be provided.

B. Computational methods

B1 The CRYSTAL program

A description of the CRYSTAL program was recently reported,[65] whereas theoretical backgrounds can be found in ref. 66 and 67 along with applications to *ab initio* modelling of solid state chemistry.

CRYSTAL is an *ab initio* periodic program which computes the electronic wave function and properties of periodic systems at the Hartree–Fock (HF) level of theory,[67] with methods derived from the density functional theory (DFT) and combining both approaches in the so-called hybrid HF/DFT techniques.[68] At variance with other common solid state *ab initio* codes like ABINIT,[69] CASTEP,[70] CPMD[71] and VASP[72] which employ either plane waves (PW) as basis set in combination with atomic pseudo-potentials to screen the core electrons or projected-augmented waves, CRYSTAL performs all-electron calculations adopting a linear combination of atom-centered Gaussian-type orbitals (GTO).

This is a peculiar feature of the code and has at least two relevant advantages and one disadvantage. Firstly, at present, hybrid HF/DFT methods represent the methods of choice in the trade-off between cost and accuracy for both molecules and solids. Indeed, the accuracy of hybrid methods, and in particular the B3LYP,[73,74] has been highlighted in a variety of studies on periodic systems (see ref. 75 and references therein). Exact HF exchange as well as hybrid functionals are standard in GTO-based solid state computer codes such as CRYSTAL, whereas, in contrast, the number of PW calculations employing hybrid functionals is still limited and problematic because of the delocalized nature of PW basis sets. Secondly, the use of GTO allows one to treat both bulk (3D) and surface (2D) structural models of HA at the same level of numerical accuracy and very efficiently. By virtue of the local nature of Gaussian functions and at variance with PW calculations, in GTO calculations the true dimensionality of the system is always obeyed, *i.e.* molecules, 2D slabs, and 3D crystals are treated without spurious effects due to artificial (for molecules and 2D slabs) replicated images. In CRYSTAL, a surface is modelled by using a thin film of a given thickness cut out from the bulk, *i.e.* a slab model. A direct and consistent comparison between bulk and surface properties (structure and vibrational frequencies) is then easily performed. As a drawback, localized basis functions suffer from the basis set superposition error (BSSE), absent for PW. BSSE may seriously affect the modelling of the adsorbate/surface interactions, particularly in the evaluation of interaction energies, which are systematically

overestimated. Nonetheless, since long ago, the Boys-Bernardi counterpoise correction[76] has been suggested as the method of choice to get rid of the BSSE and is implemented in CRYSTAL code.

Many electronic properties of crystalline systems can be computed (*e.g.* energy bands, DOSs, charge density, electrostatic potential) as well as vibrational, magnetic and dielectric properties. Among a wide variety of options, the last version of the CRYSTAL06 code[77] particularly allows to: (i) fully relax the crystalline structure through the use of analytic gradients of the energy with respect to both lattice parameters and atomic positions;[78–80] (ii) compute the vibrational frequencies at $k = 0$ (Γ point)[81] and IR intensities;[82] (iii) compute the anharmonic correction to stretching mode of X–H bonds (*e.g.* OH stretching mode).[83]

B2 The adopted Gaussian basis sets

The multi-electron wave function is described by linear combination of crystalline orbitals (CO) which, in turn, are expanded in terms of Gaussian type basis sets. For the considered cases, calcium ions have been described with the Hay-Wadt small core pseudopotential,[84,85] in which the first 10 electrons (shells 1 and 2) are represented with the effective core pseudopotential functions, while for the remaining 10 (shell orbital 3 and 4s), the basis set consists of three contracted Gaussian type functions and one GTF for the outer sp shell (basis [HAYWSC]-31G).[86] The phosphorus atom is described with the 85-21G(d) basis. Finally, oxygen and hydrogen are represented with 6-31G(d) and 31G(p) basis sets. H_2O oxygen and hydrogens were described with the same Gaussian functions used for HA surfaces. For amino acids the Pople split valence basis sets (downloadable from the CRYSTAL web site[87]) have been adopted, *i.e.* H, 31G(p); O, 6-31G(d); N, 6-21G(d); C, 6-21G(d)*, respectively.

B3 Hamiltonian and computational parameters

For all cases reported here, the B3LYP Hamiltonian was adopted, which has been used to model a large variety of crystalline systems.[88–92] Indeed, for insulating and semiconducting systems it has recently been proved that B3LYP performs better than many pure GGA functionals.[75] Furthermore, for systems in which hydrogen bond (H-bond) interactions are present, as usually happens in adsorption of molecules, in a periodic context B3LYP has been proven to perform better than PW91 as far as structure, energetics, and vibrational frequency prediction are concerned.[83,93] For frequencies of H-bonded systems in particular, PW91 has been shown to overestimate the frequency shift of the hydrogen bond donors. The same concern was recently reported by others when predicting the shift of the OH frequency of a Brønsted site in interaction with CO.[94] It is now well established that standard GGA and hybrid functionals as well are unable to cope with dispersive interactions (London forces).[95–97] Although the PW91 GGA functional apparently gives some binding for systems in which the dispersion interaction is dominant, even though for wrong reasons,[96] Becke's exchange-based methods (hybrids included) tend to be exceedingly repulsive,[98] resulting in underestimated interaction energy. Recently Grimme[99,100] has proposed a very pragmatic empirical correction which supplements the pure DFT energy term. It is based on the classical London formula in which short range and double counting of the interactions, already accounted for by DFT, are carefully avoided using a damping function. Grimme's correction is standard in CRYSTAL and the results including the dispersion contribution are supplemented by a D label (B3LYP-D, ΔE^{D}, *etc.*) in the following. Actually, some of us[101] found that the original Grimme's parameterization overestimates somehow heats of sublimation for molecular crystals and proposed a slightly different variant of Grimme's original formulation, which is the one adopted throughout this paper.

B4 Geometry optimization

Depending on the considered systems, either a full relaxation of the atomic coordinates together with the lattice parameters within the appropriate symmetry space group (HA bulk and free surfaces), or relaxation of only the internal coordinates keeping the lattice parameters fixed to the optimized values of each free surface (amino acids and water adsorption) were performed. Analytical DFT energy gradients[78,102] were used in a quasi-Newton algorithm as proposed by Schlegel[103] and implemented in CRYSTAL code.[77]

B5 Interaction energy

In a periodic treatment of adsorption phenomena, the interaction energy, ΔE, per unit cell per adsorbate molecule A (in this case, either H_2O, Gly, Glu or Lys) is a negative quantity (for a bound adsorbate) defined as

$$\Delta E = E(\mathrm{SA//SA}) - E(\mathrm{S//S}) - E_{\mathrm{M}}(\mathrm{A//A})$$

where E(SA//SA) is the energy of the optimized unitary cell containing the hydroxyapatite slab S in interaction with the adsorbate A, E(S//S) is the energy of a fully relaxed unitary cell containing the hydroxyapatite slab alone and E_{M}(A//A) is the molecular energy of the free, fully optimized adsorbate (the symbol following the double slash identifies the geometry at which the energy is computed). The above expression can also be recast to take into account the energy of deformation δE_{A} and δE_{S} due to the change in geometry upon interaction of both adsorptive and solid adsorbent, respectively. Lateral intermolecular interactions ΔE_{L} among the infinite adsorbate replicas are also computed. As the local basis set is adopted throughout all calculations, the results are known to be affected by the basis set superposition error (BSSE). As mentioned above, the same counterpoise method adopted for gas-phase intermolecular complexes[76] was adopted to correct the final interaction energy. In some cases, the interaction energy has also been supplemented to include the post-DFT dispersive term, as suggested by Grimme and implemented by some of us recently.[101] Details of the various terms which contribute to the final interaction energy have already been reported in previous publications and are not repeated here.[104]

C. How to model hydroxyapatite: from bulk to surfaces

C1 The HA bulk

Hydroxyapatite (HA, $[Ca_{10}(PO_4)_6(OH_2)]$) belongs to the crystal family of calcium apatites and can be found in nature in two different phases,[105] hexagonal and monoclinic, the latter probably associated with the stoichiometric HA.[106] The hexagonal form is the one on which all calculations presented here for bulk and derived surfaces were carried out. This form is the most frequently encountered and is involved in bone formation because it allows for much easier exchange of OH^- groups for other anions, like F^-, Cl^- and CO_3^{2-}.

The structure of the hexagonal form (see Fig. 1) has been solved within the $P6_3/m$ space group with statistically disordered OH orientation along the screw axis using X-ray[107,108] and neutron diffraction experiments.[107] From a thermodynamic point of view, the monoclinic form is the most stable. In the monoclinic phase ($b = 2a$, space group $P2_1/b$) the OH groups on the screw axis point upwards and downwards in alternate nearest neighbour columns (see ref. 109 and Fig. 2).

Quantum-mechanical simulation of the hexagonal HA cannot be performed within $P6_3/m$ space group because of the unphysical duplication of each OH group by the m mirror, so that the symmetry is reduced to $P6_3$ space group which brings all OH groups with the same alignment in each column (see Fig. 2). It is worth noting that this is also the main structural difference between monoclinic and hexagonal HA phases, all other structural features being very similar. The procedure described here was adopted in the past by other authors[107,110–112] and recently by Haverty *et al.*[64] and Tsuda and Arends.[57]

The optimized structure of hexagonal $P6_3$ HA is characterized by two formula units per cell ($Z = 2$) and contains 44 atoms per unit cell. As a consequence of the lowering of symmetry, there are three types of Ca ions inside the cell (labelled as Ca1, Ca2 and Ca3), instead of two (as in the case of $P6_3/m$ space group), in which Ca1 has three oxygen atoms as first neighbours, Ca2 six, and Ca3 four, respectively. OH group is linked to three Ca3 ions, which form an equilateral triangle in the ab plane with the hydroxyl in the centre (see Fig. 2).

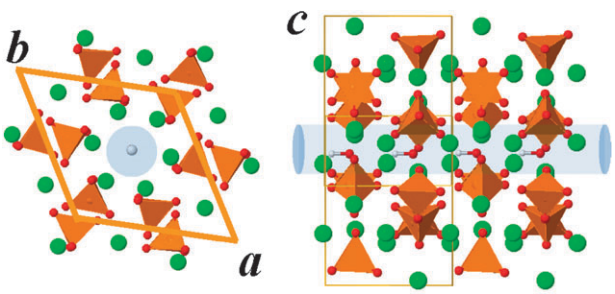

Fig. 1 Views along [001] and [110] directions and local structure around the OH groups of the hexagonal HA structure.

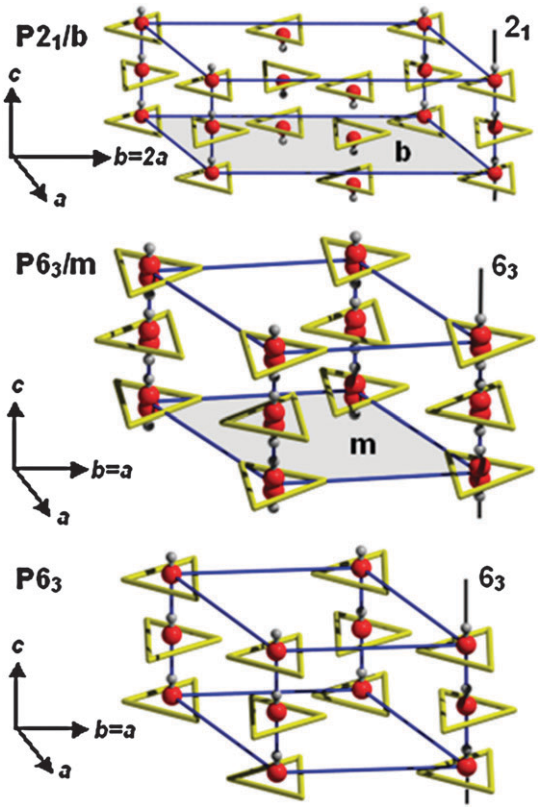

Fig. 2 Different HA structures: monoclinic $P2_1/b$ (top), experimental hexagonal $P6_3/m$ (middle) and theoretical adopted hexagonal $P6_3$ (bottom) unit cells. P, O and Ca atoms not relevant for the scheme were omitted for clarity of representation. Ca ions are at the vertices of triangles around each hydroxyl group.

Comparison between the B3LYP results and both experimental structural data[107,108] and computed ones[40,62,64] from literature reveals a very good agreement.[109] Electronic density of states and band structure analyses characterize the HA bulk as a wide gap insulator (7.9 eV) with the electronic bands practically flat. Mulliken net charges (Ca: 2.05, PO_4: −3.08 and OH: −1.02 electrons) are very close to the formal ionic charges of +2, −3 and −1 for Ca, PO_4 and OH, respectively, showing a rather ionic character of the building blocks of the HA material.

Normal modes analysis allowed for a complete assignment of the experimental IR and Raman spectral features showing an average deviation between experiment and unscaled harmonic B3LYP frequencies of about 30 cm^{-1}. Interestingly, it turned out that the adopted $P6_3$ space group brings about a phonon instability at Γ point, so that the optimized HA corresponds to a saddle point on the potential energy surface (PES) (see ref. 109 for further details). This is due to the forced OH alignment imposed by the $P6_3$ constraints and, indeed, the imaginary mode disappeared for the $P2_1/b$ HA monoclinic structure in which OH columns run in an *anti*-ferromagnetic ordering (see Fig. 2). This structure was also confirmed to be the thermodynamically most stable phase by 17 kJ mol^{-1} per unit cell. The satisfactory picture emerging from the present quantum-mechanical methodology for HA bulk allows for the treatment of the most relevant HA surfaces.

C2 The HA surfaces

To understand in detail the mechanisms of interaction between HA and the component of biological fluids, the focus should be on the structure and reactivity of HA surfaces. As already said, natural HA is found either in hexagonal or monoclinic form,[107] but only the former is relevant in terms of *biological fixation*, *i.e.* the interfacial implant/tissue bonding which is consequent to the formation of a biologically active HA layer at the implant surface.[52,113,114] The HA morphology is needle-like, as resulting from an oriented growth along the *c*-axis,[115] which is thermodynamically favoured. The HA crystal faces are responsible for the macroscopic crystal morphology as shown in Fig. 3, namely the {001}, {100} $\equiv$ {010} and {101} $\equiv$ {110} forms.

It has been observed that during bio-mineralization of teeth hard tissues (dentine and enamel) crystal growth occurs overall at the (001) plane, *i.e.* along the *c*-axis.[116,117] Still, these faces appear during the uninhibited growth of the HA crystal[118,119] and determine a morphology transformation from needles to plates, which is expected to be relevant to the formation of highly substituted crystals of bone and dentine.[120] It is clear that, because HA platelets are elongated along the *c* direction in bones and during bio-mineralization of tooth hard tissue, the {100} crystal form is the most developed, being responsible for the interaction with molecules[116,117] as shown by HRTEM studies.[121]

Although it has been observed that proteinoid layers rapidly cover HA when implanted in the body[122] and that the incorporation of the carbonate follows frequently,[116] the mechanisms of interactions between crystalline calcium phosphate and macromolecules are poorly understood, without considering the case of real and complex tissues. Many experimental efforts were carried out to gain conclusive information on the growth mechanism of the (001) face,[32,122,123] the incorporation of ions to mimic the real situation in bones,[124] and the interaction with macromolecules.[125–127] However, they lead to poor results of difficult interpretation in most cases.

To complicate further the picture, a recent HRTEM study by Sato *et al.*[121] showed that the {010} surface may be terminated just over the OH channels running along the (010) plane, giving rise to non-stoichiometric surfaces, *i.e.* those in which the formula unit of the surface unit cell cannot be expressed as an integer multiple of the formula of the HA bulk unit cell. Two different non-stoichiometric faces are ideally possible, giving rise to a different Ca/P ratio compared to the value of 1.67 for the stoichiometric cases, called Ca-rich (Ca/P = 1.71) and P-rich (Ca/P = 1.62), respectively.

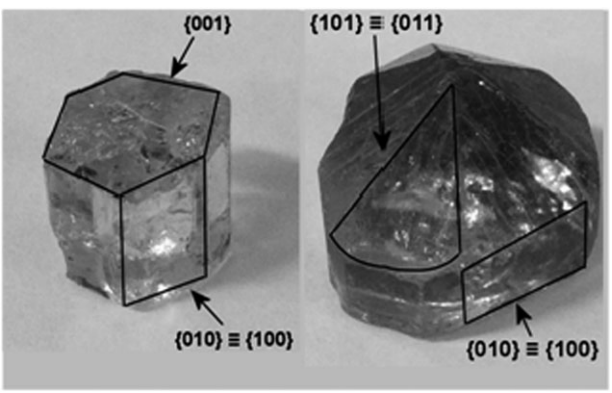

Fig. 3 Crystal forms of the hydroxyapatite mineral (crystals courtesy of Prof. P. Benna, Dip. Scienze Mineralogiche & Petrologiche, pictures courtesy of dott.ssa L. Crespi, Dip. Chimica IFM, Univ. Torino).

C2.1 The slab model and the (001) surface. Starting from the optimized HA bulk structure previously described,[109] a model of the (001) HA surface was simulated by means of the slab model. Within this model, the (*hkl*) Miller indices (in this case $h = 0$ $k = 0$ $l = 1$) and the slab thickness defined in a direction perpendicular to the (*hkl*) crystal plane family are needed. A thin film of definite thickness is then obtained, bound by two planes which may also be equivalent by symmetry. The adoption of a localized Gaussian basis set to solve the electronic problem allows to define the slab as a real 2D system (no unphysical replica of the slab along the *z* coordinate), at variance with the need for artificial replica of the pseudo slabs when adopting PW basis sets.[66] The advantage is that the wave function decays to zero at large distances above/below the upper/lower face of the defined slab, a fact that provides the rigorous definition of electrostatic potential nearby the surfaces by setting to zero the value of the potential at infinite distance from the slab. As the cut from the bulk is expected to affect the atomic positions far from the interior of the slab, full geometry relaxation (lattice parameters and internal coordinates) is usually performed. The relevance of relaxation is expected to decrease with the increase of the slab thickness. On the relaxed slab geometry, the energy needed to generate the (*hkl*) surface from the bulk, E_{surf}, is computed with the standard formula:

$$E_{surf} = (E_{sN} - N \cdot E_b)/2A$$

in which E_{sN}, N, E_b and A are the energy of the slab unit cell, the number of bulk unit cell present in each considered slab model, the energy of the bulk and the unit cell area (constant for each slab), respectively. The factor 2 accounts for the presence of two surfaces for each slab. The minimal thickness which can be considered representative of the {001} form was found to be 13.5 Å (called double-layer) giving $E_{surf} = 1.043$ J m^{-2} envisaging a structure which consists of 88 atoms in the unit cell[128] as shown in Fig. 4, section I.

In the slab, compared with the bulk geometry, the surface Ca ions move inwards to shield their charges, by about 0.25 Å for each face.

C2.1.1 Electrical peculiarities of the (001) HA surface. As quoted before, E_{surf} (as well as other properties like band gap, net charges *etc.*) should converge to a stable value as a function of the slab thickness. The high cost of the B3LYP full optimization for thicker slabs prevents the adoption of a straightforward approach to assess the convergence by simply increasing the slab thickness and relaxing the geometry of the given slab. For the (001) HA surface, this is a particularly serious drawback because, as shown in Fig. 4, it exhibits ferro-electricity owing to the alignment of the OH groups along the *z* slab axis. In principle, the ferroelectric alignment

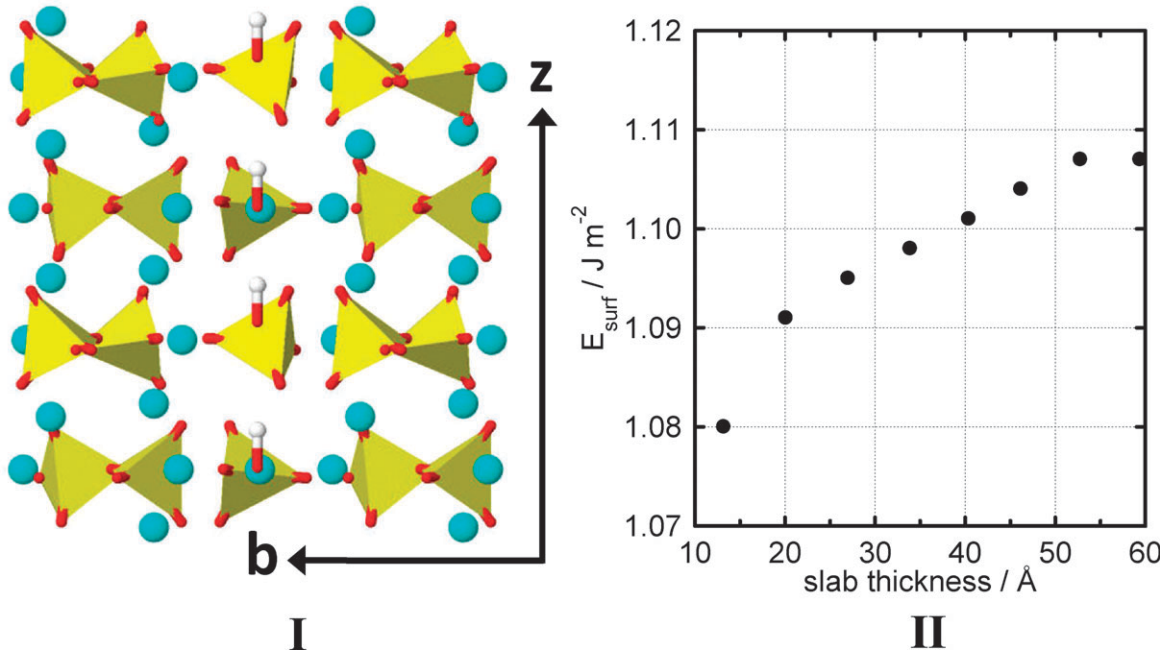

Fig. 4 Section I: view along the [100] direction of the HA (001) slab model. Colour coding: Ca ions (light blue), H (light grey), O (red), PO_4 groups as yellow tetrahedra. Section II: E_{surf} as a function of the HA (001) slab thickness.

may render the electronic structure of the slab unstable as a function of the slab thickness, because the resulting macroscopic dipole across the slab would bend the electronic bands with a catastrophic behaviour. To investigate this point, we rely on molecular mechanics (MM) relaxation of the geometry of slabs of different thickness (GULP code[129]), using a recently developed shell-ion model potential[130] devoted to model HA. On each optimized MM slab a B3LYP single point energy calculation was carried out and the surface energy E_{surf} computed accordingly. The same procedure was followed for the (001) surface slabs derived from the HA monoclinic phase, in which the OH columns run in an antiparallel fashion, thus imparting an *anti*-ferroelectric character to the (001) face and resulting in a null dipole across the slab. The thickest considered HA hexagonal slab was a nona-layer (396 atoms in the unit cell, 60 Å thick), whereas for the monoclinic case whose unit cell is doubled compared with the hexagonal case, the thickest considered slab was a tetra-layer (352 atoms in the unit cell, 27 Å thick).

The resulting B3LYP E_{surf} values for the hexagonal case (see Fig. 4 section II) show a slow increase with the slab thickness. For the monoclinic *anti*-ferroelectric phase, a value of 1.337 J m^{-2} was computed irrespective of the slab thickness. The gentle E_{surf} increase parallels the closure of the band gap (from 7.7 to 4.8 eV) which will inevitably bring the (001) HA hexagonal surface band structure to collapse for thicker slabs. Analysis of the data (see ref. 128 for details) reveals that this may happen for slabs of relatively large thickness, probably of the order of 10 nm. The presence of the macroscopic dipole due to the ferroelectric OH alignment is the reason for the increase of E_{surf} value with the slab thickness. The present results prove, however, that the (001) HA slab can contrast this electric field, because the electronic structure generates a field converging to a finite value.[131,132] Indeed, the average electric field $\langle E \rangle$ computed as:

$$\langle E \rangle = (\mathrm{Vu}-\mathrm{Vb})/(\mathrm{zu}-\mathrm{zb})$$

in which Vu and Vb are the electrostatic potential values 2 Å away from the topmost (Vu, zu) and lowest (Vb, zb) Ca ion at the surface, converges rapidly to a constant value as the thickness increases, thus ensuring a non-catastrophic behaviour[133] in the electronic structure.

The presence of the field across the slab suggests that for the real material, when the slab thickness becomes very large, the system would probably prefer to either go to some protonic disorder within the same OH column (OH flip-flop) or to reorganize in domains of monoclinic phase (*anti*-ferroelectric OH organization). That the OH flip-flop can annihilate the macroscopic electric field is seen from the electrostatic potential maps mapped on an electron density surface of constant value for the top/bottom faces of the HA (001) surface shown in Fig. 5. The upper maps (Fig. 5-I) are relative to the pristine (001) HA surface and the top/bottom maps exhibit different electrical features due to the OH ferroelectric alignment.

For instance, the central region of the top map is almost positive-valued due to the terminal H atom of the OH column, whereas for the bottom map it is entirely of negative-value because of the terminal O atom of the OH column. In agreement with the finite dipole across the slab, the bottom map appears of more negative-value than the top one. The maps of Fig. 5-II have been computed for the same (001) HA slab in which the two top-most OH groups of each column have been flipped by 180°. In this way a "defective" OH···HO moiety is formed in the middle of the slab (the two OH are slightly bent with respect to the *z*-direction, to reduce mutual

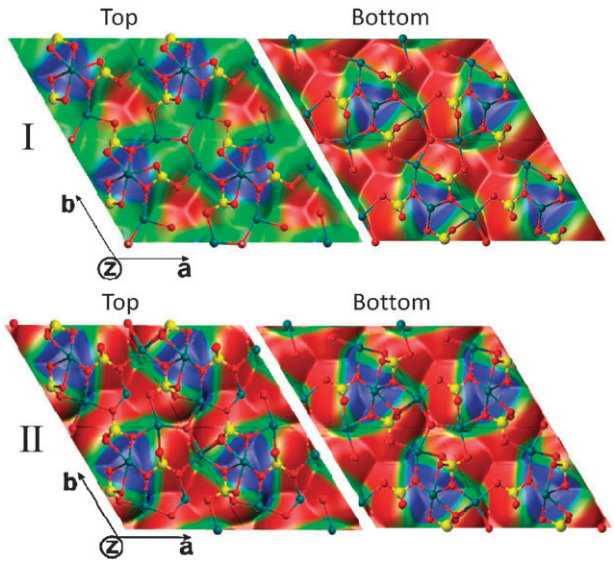

Fig. 5 Top/bottom view along the [001] direction of the electrostatic potential of HA (001) (I) and HA (001)-*anti*-OH (II) slabs mapped on a surface of constant electron density (10^{-6} a.u.). For clarity, four unit cells have been reported. Colour coding for atoms: oxygen (red), calcium (cyan), phosphorous (yellow), hydrogen (grey). Positive/negative values of the electrostatic potential (±0.02 a.u.) as blue/red colours.

H···H repulsion), so that the macroscopic dipole disappears. Indeed, the symmetry in the electrostatic features of the maps is now completely restored and the E_{surf} is 1.058 J m^{-2}, by 0.015 J m^{-2} higher than the value of the polar (001) face.

Interestingly, the electrostatic features of the double-layer are already very close to the limiting value computed for the nona-layer so the former can be adopted as the slab of reference to represent the HA (001) surface in adsorption processes. The interested reader can refer to our recent work,[128] in which convincing evidence was provided in that respect.

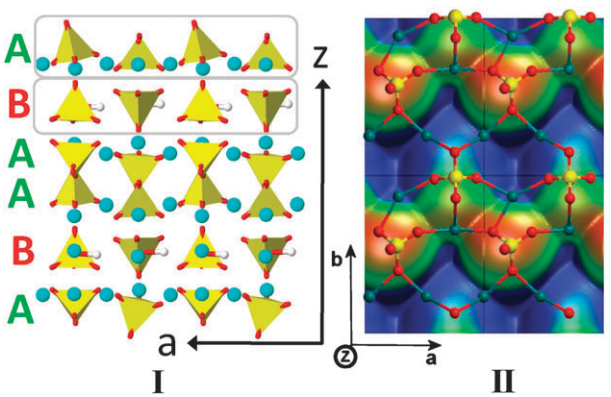

Fig. 6 Section I: view along the [010] direction of the HA (010) slab model. A-type layers envisage $Ca_3(PO_4)_2$ composition, B-type layers $Ca_4(PO_4)_2(OH)_2$. Colour coding: Ca ions (light blue), H (light grey), O (red), PO_4 groups as yellow tetrahedra. Section II: electrostatic potential mapped on a surface of constant electron density (10^{-6} a.u.). Colour coding for atoms: oxygen (red), calcium (cyan), phosphorous (yellow), hydrogen (grey). Positive/negative values of the electrostatic potential (±0.02 a.u.) as blue/red colours.

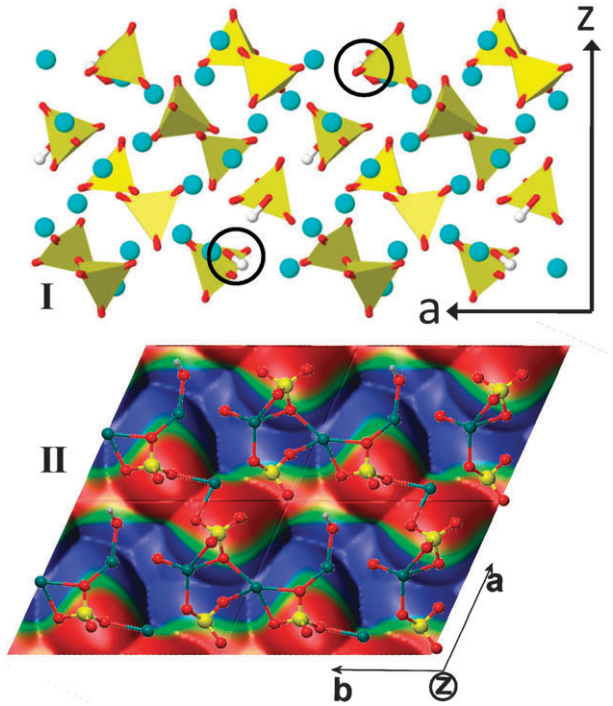

Fig. 7 Section I: view along the [010] direction of the HA (101) slab model. Colour coding: Ca ions (light blue), H (light grey), O (red), PO_4 groups as yellow tetrahedra. Section II: electrostatic potential mapped on a surface of constant electron density (10^{-6} a.u.). Colour coding for atoms: oxygen (red), calcium (cyan), phosphorous (yellow), hydrogen (grey). Positive/negative values of the electrostatic potential (±0.02 a.u.) as blue/red colours.

C2.2 The (010) and (101) surfaces. Fig. 6 and 7 illustrate the B3LYP optimized structures and the electrostatic potential maps for the HA (010) and (101) model slabs, respectively.

The (010) face envisages alternating electro-neutral layers of $Ca_3(PO_4)_2$ (A-type) and $Ca_4(PO_4)_2(OH)_2$ (B-type) obeying the A–B–A–A–B–A sequence. OH channels run parallel to the (010) plane resulting in a non-polar slab with the E_{surf} value higher than the (001) case (1.709 *vs.* 1.043 J m^{-2}). The B3LYP electrostatic potential map shows interconnected bands of strongly positive potential (blue color) divided by corresponding ones of negative values (red color). It is then expected that the local polarity at the (010) surface will exert a powerful action on dipolar molecules like water or amino acids. Mulliken net charges of the atoms nearby the surface are very close to the stoichiometric values (Ca^{2+}, OH^- and PO_4^{3-}) confirming the ionic nature of the material. This face is rather extended in the HA morphology so it will play a key role in adsorption (see Fig. 3). Indeed, in the mineral phase of bones, due to the alignment of the *c* axis of HA platelets with the collagen, a key role of the (010) face is expected in modulating the interaction with proline and hydroxyl-proline of the collagen rod.

Fig. 7 shows the case of the (101) surface: the pristine surface resulting from the geometrical cut of the bulk exhibits OH groups running diagonally across the slab and giving rise to a macroscopic electric dipole moment across the surface. Geometry relaxation, however, reduces the macroscopic dipole by rotating the two terminal OH groups (highlighted

by circles in Fig. 7-I) bringing the E_{surf} to 1.646 J m^{-2}, with a slightly better stability compared with the (010) case. The electrostatic potential map (Fig. 7-II) reveals similar features to those already discussed for the (010) case, so that its behaviour with adsorbates is expected to be similar.

C2.3 Non-stoichiometric (010) surfaces. A recent HRTEM study by Sato *et al.*[121] highlighted peculiar terminations of the (010) surface in which the surface was terminated just over the OH channels (running parallel to the surface) giving rise to the so-called Ca-rich (010) non-stoichiometric surface. Fig. 8 shows both the Ca-rich (B–AA–B–AA–B, Ca/P = 1.71, section I) and the corresponding P-rich (AA–B–AA–B–AA, Ca/P = 1.62, section II) structures as resulting from the B3LYP optimization. Careful handling of the positions of the surface Ca ions ensured that both surfaces were electroneutral and non-polar. Clearly, due to the non-stoichiometric nature, E_{surf} cannot be defined using the classical formula (*vide supra*). Astala and Stott[38] adopted a clever and rather involved scheme to evaluate the phase existence conditions for the two non-stoichiometric surfaces, showing that the region of their stability is outside the stability window defined by bulk HA, $Ca(OH)_2$ and β-tricalcium phosphate, respectively. Electrostatic potential maps (see Fig. 8) reveal a higher nucleophilic character of the Ca-rich as compared to the P-rich, so that a higher activity of the former is expected when adsorption of molecules will be considered.

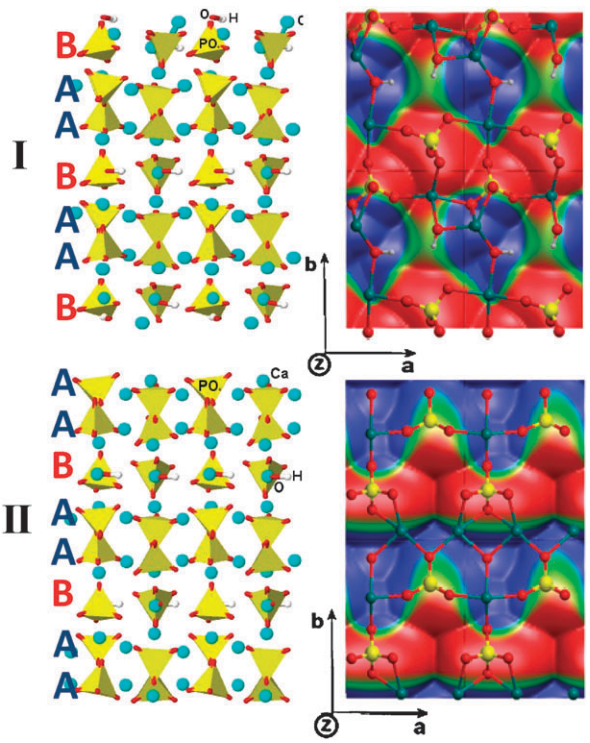

Fig. 8 Section I left: view along the [010] direction of the non-stoichiometric Ca-rich HA (010) slab model. Colour coding: Ca ions (light blue), H (light grey), O (red), PO_4 groups as yellow tetrahedra. Section I right: electrostatic potential mapped on a surface of constant electron density (10^{-6} a.u.). Colour coding for atoms: oxygen (red), calcium (cyan), phosphorus (yellow), hydrogen (grey). Positive/negative values of the electrostatic potential (±0.02 a.u.) as blue/red colours. Section II: same as section I but for the P-rich HA (010) slab model.

In summary, the present results demonstrate that the chemical behaviour of all considered surfaces is the behaviour expected for an ionic material, in which rather strong electric fields are present nearby the surface ions (Ca^{2+} and PO_4^{3-}). This, in turn, will strongly influence the adsorption of biomolecules, which have, in almost all cases, a strong polar nature. The added value of the straightforward evaluation of the quantum-mechanical electrostatic potential is beneficial in our understanding of the key processes occurring on the HA surfaces: in all cases one cannot reduce their nature to simple models based, for instance, on the existence of exposed Ca cations (believing in a strongly positive surface) because regions of strongly negative potentials are equally relevant in dictating the adsorption processes. As we will see in the next paragraphs this point is a key one to understand the structural, energetic and vibrational features of water and amino acids adsorption.

D. Hydroxyapatite surfaces in interaction with water: a molecular or chemisorption process?

Water is ubiquitously present in the biological fluids as life itself is not sustainable without its peculiar properties. So, the interaction of the surface with water molecules dominates the initial contact of whichever biomaterial with the bio-world, *i.e.* the living matter components. Water molecules are rapidly adsorbed at the solid surface and form a mono- or bi-layer whose structure is expected to be quite different from that of the liquid water since it is strongly affected by the nature/structure of the underlying surface.[19,134–139] For these reasons it is extremely important to understand the details of how water will be adsorbed on the HA crystal faces discussed above.

Two problems arise to achieve this goal: (i) how to set up a physically sound initial geometrical guess and (ii) how many water molecules per surface unit cell can a given surface accommodate. Point (i) can be easily tackled by following the indications from the electrostatic potential maps of the bare surfaces previously discussed (*vide supra*). By adopting the principle of complementarity between adsorbate/adsorbent electric features, the negative region of the electrostatic potential of water (around the oxygen lone pairs) will face the most positive region of the considered surface, which are obviously those where the most exposed Ca ions are located. Geometry optimization will also allow for more subtle interactions to occur, like H-bonds between water H atoms and the negative regions of nearby PO_4 groups (the reader may return to a quick look at the electrostatic maps of the previous paragraph). As for point (ii) one can iterate the procedure of point (i) for all surface Ca ions to a point in which all of them become engaged in interaction with water molecules.

The key question here is to assess if water molecules will adsorb at the HA surface sites molecularly or in a dissociative way. Indeed, at the surface of an inorganic material H_2O molecules may adsorb through different mechanisms, according to the nature and distribution of reactive surface sites.[140] On surfaces exposing reactive sites, water molecules

are dissociatively adsorbed giving rise to a hydroxylated (OH-terminated) layer. This happens generally when the material has been thermally or chemically activated, or has been irradiated. The nature of these reactive sites depends upon the chemical properties of the material, in particular on the ionic or covalent character of its surface. In the former case, H_2O is dissociated at coordinatively unsaturated cation–anion pairs located at kinks, edges and steps of nanocrystal faces (*e.g.* MgO, Al_2O_3, TiO_2), whereas, in the latter case, H_2O is dissociated on strained moieties, such as for instance SiOSi bridges in silica. Conversely, on flat surfaces of ionic materials, H_2O is still strongly bound at coordinatively unsaturated cations but as intact, non-dissociated molecules. On hydroxylated surfaces water molecules can be bound (still more strongly than in liquid water) through a network of H-bonding. All these surfaces can be classified as hydrophilic, *i.e.* wetting surfaces. It is worth noticing that often all these processes occur in different regions of the same surface or on different faces of a same crystalline material, as a consequence of the well known heterogeneity of a 'real' surface. On another kind of surface, by contrast, the water–surface bond is weaker than the H-bonds in liquid water and this kind of surface is considered as hydrophobic, in that non-wetting. The energetic discrimination between hydrophilic/hydrophobic surfaces is based on the binding strength of water to the surface at a molecular scale.[140–142] All this is extremely relevant in investigating the role of water in biology and, in particular, the interplay of water–biopolymer and surface–biopolymer interactions.[139] The competition/synergy between hydrophilic and hydrophobic interactions can be crucial in determining, for instance, the adsorption of a protein at the biomaterial surface. Further, the possibility that water is dissociatively adsorbed, so inducing an irreversible modification of the surface structure, may play a key role for its contact with body fluids and biopolymers.[23]

In the following, the case in which adsorbed water maintains its molecular integrity will be first considered followed by the case in which water is dissociatively adsorbed. We will start by adsorbing one water molecule, in order to mimic the first contact of the surface with an individual molecule and then by considering the adsorption of a number of molecules sufficient to reach, for the (001) and (010) HA surfaces, a coverage simulating the monolayer of adsorbed water.

D1 Non-dissociative adsorption of a single water on HA surfaces

The case in which a single water molecule remains molecularly adsorbed at the (001), (010), (101), (010) Ca-rich and (010) P-rich is shown in Fig. 9.

In all cases, water was initially placed on the most exposed Ca ion (on both up/down surfaces of each slab to avoid distortions in the electronic density). Water interacts with oxygen down with the Ca ions (average distance around 2.3 Å) and makes H-bond with the nearby surface oxygens belonging either to the PO_4 group or, for the (010) Ca-rich case only, to the surface OH group. The strength of H-bond is rather variable as can be judged by both geometrical and vibrational features: the $H_w\cdots O_{surf}$ distances are 1.51, 1.59, 1.86, 1.72 and 1.92 Å for the (001), (101), (010), (010) Ca-rich and (010) P-rich surfaces, respectively. These values are perfectly parallel to the B3LYP bathochromic shift in the symmetric OH stretching mode of the adsorbed water compared to the value for the free molecule, resulting in shifts of 1165, 1071, 337, 761 and 329 cm^{-1}, respectively. The bending mode suffers, as expected, a hypsochromic shift caused by the increased hindering of the H–O–H angle due to the engagement with the surface: the average shift is around 100 cm^{-1}, which can be considered a rather strong perturbation. These data are quite remarkable: water is strongly perturbed but, nevertheless, it remains molecularly adsorbed. Indeed, any attempt to de-protonate water for the most favourable case (the HA(001) surface) by manually attaching one proton to the PO surface bond did not bring about a stable structure, as the proton jumps back from the surface to the OH fragment to restore the water molecule.

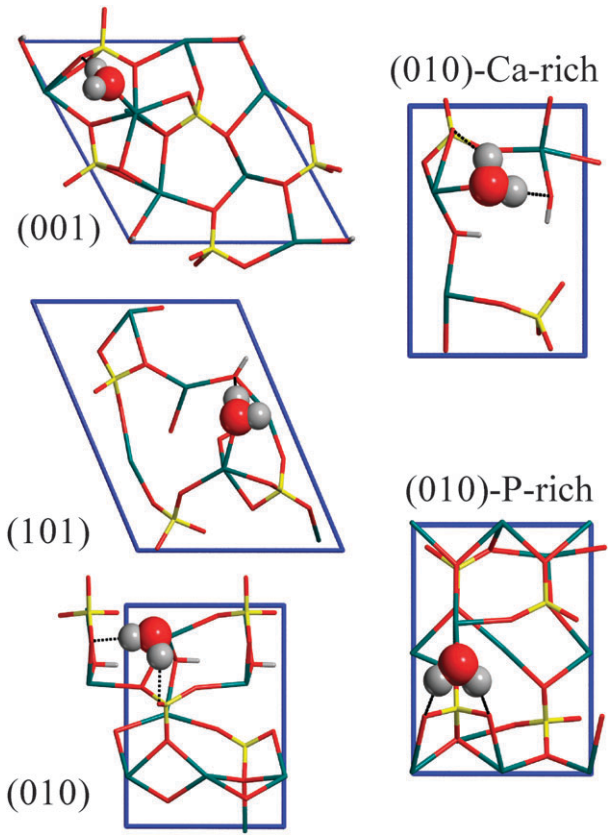

Fig. 9 View along the *z*-axis of the HA slab models interacting with a single water molecule.

Table 1 Energetic contributions to the heat of adsorption $-\Delta_a H(298)$ for single water molecule molecularly adsorbed on the HA surfaces. All data in kJ mol^{-1}

Surfaces	δE_S	δE_W	ΔE_W	ΔE_L	BE^{*C}	BE^{CD}	$-\Delta_a H(298)$
(001)	30	7	8	−0.7	138.4	110.1	98.9
(101)	31	4	5	−0.4	164.6	146.6	133.5
(010)	15	2	2	−0.6	137.7	135.6	121.3
(010) Ca-rich	19	4	5	−0.8	139.8	130.9	117.2
(010) P-rich	8	3	3	0.0	122.6	125.0	109.8

Energetic data are shown in Table 1. The meaning of the symbols can be found in the Computational details section.

The BE^{CD} represents the B3LYP electronic binding energy which has been corrected for BSSE (being, as average, around 35% of the uncorrected BE) and for dispersive contribution not accounted for by B3LYP by Grimme's formulation, as encoded in CRYSTAL. The final heat of adsorption, $\Delta_a H(298)$, has been computed by using the intermolecular vibrational modes plus those of water to correct the electronic energy. As a general remark, water interacts rather strongly as testified by both the relatively high geometry deformation cost suffered by the HA surface (first column δE_S) and by the average heat of adsorption being, for all cases, around 120 kJ mol^{-1}.

D2 Dissociative adsorption of a single water on HA surfaces

Considering the variability and complexity (both in shape and in values) of the electrostatic potential at the different surfaces it would be interesting to assess whether water can be dissociated by adsorption on specific sites of the considered faces. For the (001) surface this has been proved to never occur. For the (010) and (101) surfaces, three out of four Ca ions are able to adsorb water dissociatively. For the latter case, a complex reconstruction is operated by water (details will be the subject of a future work).[143] The most interesting case is for the (010) surface, as illustrated on Fig. 10: Ca1 is the only site where water sits molecularly (illustrated in the previous paragraph), whereas for both Ca2 (A and B) and Ca3 it dissociates during geometry optimization, the OH group being shared by three Ca surface ions and the proton being attached to a P═O bond.

It has been argued[104] that the driving force for the spontaneous water dissociation is due to the proper arrangement of the OH^- anion, which becomes coordinated by three surface Ca ions (Ca2A, Ca2B and Ca3) with a local geometry resembling that of the structural OH groups within the HA channels (see Fig. 1). Indeed, when water is adsorbed on Ca1 it maintains its molecular nature, because the final OH^- arrangement is hindered by the unfavourable geometrical features. For Ca2 (both sites) a similar but more strained final structure is formed as shown in Fig. 10 and by the reaction energy of adsorption, −249 kJ mol^{-1}, less negative than −315 kJ mol^{-1} for H_2O on Ca3 site. For the (101) surface the reaction energy is still large, −192 kJ mol^{-1}, but definitely less so, probably because of the complex structural reconstruction needed to dissociate water. The present data have been carefully checked for systematic errors in our own methodology and are confirmed by the independent study by Astala and Stott[38] using PBE functional and the SIESTA code.[144] These computed values are so high that when considering the real HA material, which has usually been grown in aqueous environment, the question whether the unreconstructed (010) surface exists as such remains. Nevertheless, in the following, we considered both the "as cut" (010) and the "reconstructed by water" (010)-RW surfaces for modelling adsorption, as a number of experiments are carried out on HA sample pre-treated at temperature high enough to remove the reacted water from the surface. Obviously, the (010)-RW surface will behave as a softer acid/base surface compared to the un-reacted (010) one, as its most active sites were already engaged by the reaction with water.

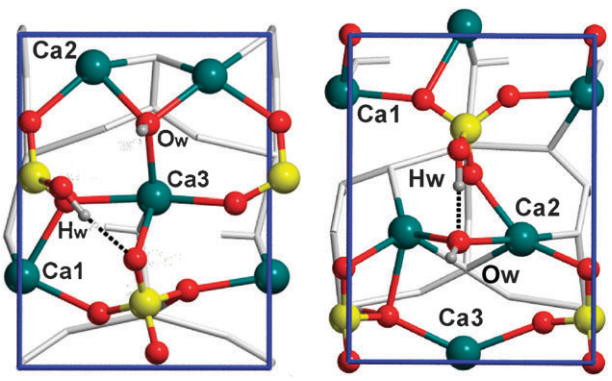

Fig. 10 Optimum structures for H_2O chemisorption on the HA (010) surface with H_2O initially adsorbed on: Ca3 (left) and Ca2 (right) cations, respectively. H-bonds as dotted lines. The new functionalities resulting by the reaction with water have been labelled Ow and Hw respectively.

D3 Water adsorption on HA surfaces: higher loadings

A key question is to see whether the chemical behaviour of the main HA surfaces is changing as a function of an increasing water loading. For instance, would a higher water loading promote further dissociation of the adsorbed water or, perhaps, would the lateral interactions (H-bonds) between adsorbed water molecules become dominant? Table 2 and 3 show the results of the B3LYP simulation: Wn refers to the total number of adsorbed water molecules, including the adsorbed molecules on the top/bottom surfaces. So, for instance, W2 means one water molecule per face inside the surface unit cell, considering the two available faces. For the (001) surface the highest coverage envisages 5 water molecules per face unit cell/surface.

For the (010) surface, only the "reconstructed by water" (010)-RW surface was considered, a choice justified by the arguments of the previous paragraph (*vide supra*). For all considered coverages, no further water dissociations resulted for both surfaces. This is a remarkable result, particularly for the (010)-RW surface which behaves similarly as far as the heat of adsorption to the less reactive (001) surface is concerned. Fig. 11 shows the structures of the two surfaces with the highest water loading.

For the (001) case, water molecules enjoy mutual H-bonds whose H···O distances (1.9 Å as an average) indicate a network of moderate strength. Beside one water molecule making a rather short H-bond with the P═O group of the

Table 2 Energetic contributions to the heat of adsorption $-\Delta_a H(298)$ for high loading of water molecularly adsorbed on the HA (001) surface. Data in kJ mol^{-1}

(001)	δE_S	δE_W	ΔE_W	$\Delta E_L{}^C$	BE^{*C}	BE^{CD}	$-\Delta_a H(298)$
W2/Ca1	30	7	8	0.0	138.4	109.3	98.1
W4	23	1	9	−3.4	103.5	89.7	75.9
W8	15	2	2	−13.0	73.3	86.5	70.1
W10	19	4	5	−15.9	63.4	85.8	68.5

Table 3 Energetic contributions to the heat of adsorption $-\Delta_a H(298)$ for high loading of water molecularly adsorbed on the HA (010)-RW water-"reconstructed by water" surface. Data in kJ mol^{-1}

(010)-RW	δE_S	δE_W	ΔE_W	$\Delta E_L{}^C$	BE*^{C}	BE^{CD}	$-\Delta_a H(298)$
W2/Ca1	26	7	6	0.0	123.9	113.2	102.2
W4	25	−3	6	−3.5	110.0	99.7	85.9
W6	23	−11	3	−8.0	88.0	86.5	71.0
W8	22	−11	3	−4.2	79.6	75.6	58.6

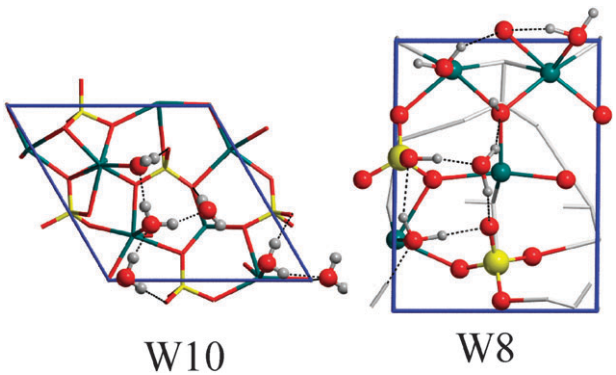

Fig. 11 Views of the surface unit cells (top surface face) for the HA (001) (W10) and (010)-RW (W8) cases. H-bonds as dotted lines.

surface (H···O of 1.41 Å) the remaining water molecules are loosely bound to the HA surface. This trend is enhanced by the increasing water loading, as the data of Table 2 nicely show. Indeed the surface deformation term δE_S decreases whereas the lateral interaction energy between water molecules, $\Delta E_L{}^C$ increases (on an absolute scale), in agreement with the geometrical results. As a whole, the final heat of adsorption $\Delta_a H(298)$ decreases for higher water loading.

A different pattern is computed for the (010)-RW case: here the surface deformation term δE_S remains almost constant as the lateral interactions are much smaller than for the (001) surface. Checking the (010)-RW structure of Fig. 11 it is seen that, at variance with the (001) case, the adsorbed water molecules never directly interact with each other but always through a surface P═O group. In the end, however, both cases display comparable values of the heats of adsorption.

The present methodology also provides a trace of the perturbation suffered by water molecules by comparing the vibrational spectrum of free water molecules with that of adsorbed water. Results of the calculations[104] show an average bathochromic shift suffered by the OH stretching frequency of about 400 cm^{-1}, with outliners in which the shift can be as large as 1200–1400 cm^{-1}. The same strong perturbation is also undergone by the HOH bending mode, whose average ipsochromic shift is around 80 cm^{-1}. Remarkably, both are in agreement with the experimental measurements.[145]

A further check of the validity of the present approach is given by the good agreement shown by the computed energetic data with the experimental heats of adsorption, which were obtained, in parallel with computational work, through direct gas/solid microcalorimetric measurements on a nanosized HA specimen (see ref. 104 for details), following a well-established stepwise procedure (ref. 16 and references therein).

In Fig. 12 experimental equilibrium adsorption enthalpies are reported as a function of increasing water coverage, expressed as the number of adsorbed molecules per number of Ca surface cations and are contrasted with the B3LYP $-\Delta_a H(298)$ values obtained, for all considered surfaces, at the indicated water coverage. Latent heat of liquefaction of water is also indicated as boundary line for discriminating hydrophilic and hydrophobic interactions.[23,136,140] The shape of the curve (which relies on the experimental heat values obtained for the surface in equilibrium with water vapour) depends on, and actually describes, the heterogeneity of surface sites.[16] Experimental heats of adsorption represent, at any specific coverage, a reasonable measure of the energy of interaction of H_2O with individual sites, whereas the extrapolated to-vanishing-coverage value $[-(\Delta_a H)_0]$ represents the enthalpy change associated with uptake on the most energetic sites, which are expected to be active in the earliest stages of the adsorption process. The extrapolated quantity of experimental origin can be conveniently compared with the interaction energy of one water molecule with an individual model site, as obtained through *ab initio* calculations. B3LYP $-\Delta_a H(298)$ values reported in the plot are the ones obtained for the non dissociative (101) and (001) crystal faces as well as for the, still non dissociative, water-reconstructed (010)-RW face (*vide supra*). Data for two non-stoichiometric HA, the (010) Ca-rich and (010) P-rich ones, are also shown for comparison purposes, as a recent HRTEM study by Sato *et al.*[121] highlighted these peculiar terminations of the (010) surface. The choice to compare the "reconstructed by water" (010)-RW face instead of the "as cut" (010) was due to the feeling that this latter face is so highly reactive toward water (BE > 300 kJ mol^{-1}, *vide supra*) that we believe that this face hardly exists as such in real HA systems grown in aqueous

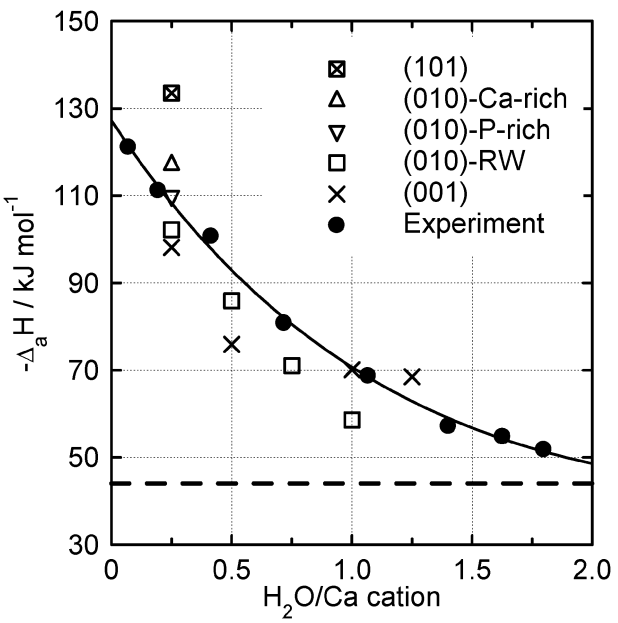

Fig. 12 Water enthalpy of adsorption as a function of water coverage. Micro-calorimetric measurement on a hydroxyapatite nano-sized specimen (filled circles); B3LYP $-\Delta_a H(298)$ values, for all considered surfaces. Enthalpy of liquefaction of water as dashed line.

medium by dropping a solution of H_3PO_4 in a $Ca(OH)_2$ suspension. Still, the vacuum activation of the HA surface (T = 573 K, $p \leq 10^{-5}$ Torr) was not sufficiently severe to remove the irreversibly bound dissociated water.

Before describing the quantitative details of the plot, it is worth noticing that the general agreement between the computed and measured $-\Delta_a H$ values is remarkable at both low and high coverage, for all considered surfaces. This is particularly true if we consider that: (i) B3LYP data for high water loading have been obtained only on two crystallographic defined surfaces, (001) and (010)-RW, whereas the experiments were performed on a polycrystalline nanosized sample, for which neither the distribution of different crystal faces nor the population of possible structural/chemical defects were well defined; (ii) the simulated models at high θ are simple microstates on a purely electronic potential energy surface, in that no thermal effects have been included.

This latter issue is particularly serious and only *ab initio* molecular dynamics would be able to provide a sensible picture of the water adsorption at room temperature. At this point, results from the present approach can be safely considered as a starting point in a more thorough analysis inclusive of the dynamic effects which is a project undertaken recently in our laboratory.

Experimental enthalpy decreases from a rather high zero-coverage value [$(-\Delta_a H)_0 > 120$ kJ mol^{-1}] down to $\sim$50 kJ mol^{-1} eventually approaching the heat of liquefaction of water [$-\Delta_L H$ = 44 kJ mol^{-1}]. By a further inspection of Fig. 12 it is clearly evident that the energy of the water/surface sites interaction is initially quite high: the comparison between experimental and computed enthalpy data is straightforward in that the adsorption of water on this particular nanosized HA sample was confirmed to be molecular in nature by IR spectroscopy (as reported and extensively discussed in ref. 145) However, in spite of the molecular nature of the interaction, a fraction of adsorbed water (*ca*. 30% of the total uptake) was not removed by RT evacuation (see ref. 104 for details).

The fact that water interacts rather strongly is also testified by both the relatively high geometry deformation cost suffered by the HA surface (*vide supra*, Table 2 and 3) and by the high heat of adsorption ($120 < -\Delta_a H < 70$ kJ mol^{-1}) measured for the edification of the monolayer on Ca sites and the average computed heat of adsorption ($\sim$120 kJ mol^{-1}). By inspecting in detail the computed values reported in Fig. 12, it can be noticed that at very low coverage the heat of adsorption for the (101) and the non-stoichiometric (010) surfaces is rather high ($>$120 kJ mol^{-1}). However, it is worth recalling that the (101) face is not the dominant feature in the HA morphology (see Fig. 3), whereas the relevance and extension of the non-stoichiometric (010) surfaces is, at the moment, debatable.

At first sight, it could be thought that such a strong interaction of molecular water could be a precursor of a dissociative adsorption, as would be expected in the case of thermally activated ionic oxides,[140] but this was not the case, in spite of the ionic character of HA. This is most likely due to the nature of the negative counterions of Ca^{2+} cations in HA (covalent PO_4^{3-} groups), with respect to the basic O^{2-} moieties present in metal oxides, characterized by well known high reactivity.

In fact, the reasons for such strong affinity to water stem most likely from the synergy between *cus* Ca ions and PO_4 species located in close vicinity. This is confirmed by the B3LYP optimized structures (see discussion above, Fig. 11 and ref. 104) in which strong H-bonds with the PO_4 species give an extra stabilization to H_2O molecules coordinated on *cus* Ca ion sites.

As far as a high coverage is reached, the inspection of Fig. 12 indicates that the experimental heat of adsorpion approaches 44 kJ mol^{-1} (latent heat of liquefaction of water) only after a second water molecule has been adsorbed (as average) per Ca ion, *i.e*. after a bilayer of adsorbed water has been accomplished. This means that the H-bond interactions responsible for the adsorption of water in the second layer are still stronger than those experienced by H_2O molecules in the liquid. This effect, which has been observed to be still more evident in the case of Mg-substituted HA,[35] is most likely due to the strong polarization of the first-layer water adsorbed molecules.

Indeed, at high coverage (more than one molecule per Ca ion) the $-\Delta_a H(298)$ of water adsorbed on the (001) surface turns out to be larger than for the (010) one, and seems to reach a plateau. This is in agreement with the onset (at high θ) of lateral interactions among the molecules adsorbed on the (001) surface, which causes the $\Delta E_L{}^C$ (*vide supra*) among the adsorbed moieties to contribute significantly to the heat of adsorption (see Table 2 and 3 and previous discussion). This does not occur on the (010)-RW surface in which water molecules, even at high θ, interact *via* H-bond with surface P═O, POH or OH groups rather than with the other adsorbed water molecules.

E. From water to biomolecules: the gas-phase adsorption of glycine, glutamic acid and lysine on hydroxyapatite surfaces

As we have already pointed out, teeth and bones are constantly in contact with body fluids and in particular with bio-macromolecules. Also the integration of a bioglass implant in a body is crucially mediated by the interaction occurring between the body fluids and the thin layer of HA formed at the surface of the material. The detailed knowledge of the microscopic steps which bring water, ions and bio-macromolecules into play on the HA surfaces is out of the possibilities of the present (and near future) *in silico* quantum-mechanical simulations. Nevertheless, the final purpose of simulation is not to mimic nature in all its fine details, but rather to understand the key steps which are essential for the functioning of the complex chain of biochemical events occurring in any living organism. For this, one essential ingredient of modern simulation is to design model systems which can be used to highlight selective behaviour of the whole and exceedingly complex system. This is exactly the case here, in which the focus is on understanding protein/HA interactions. In principle, water should be included in the simulation, to solvate both protein and HA surfaces (*vide supra*). Furthermore, simulation should also explore the conformational changes, if any, undergone by the protein when approaching

the HA surfaces, followed by a complex desolvation process of both the wet HA surface and the protein itself.[23] A more feasible and still physically sound approach would be to first study protein building blocks, *i.e.* amino acids, without the interplay of water. This can be thought of as the minimal model possible which leads to the understanding of the fundamental interactions taking place among different functionalities exhibited by the various amino acids. Within the reductionistic approach, it is believed that what one can learn from single building blocks can then be transferred, of course with some care, to describe the behaviour of the whole protein.

For that purpose the adsorption data of three amino acids on HA surfaces under strict gas-phase conditions are reported. It may be surprising that amino acids can indeed be easily sublimated without decomposition and their spectral features measured by FTIR with great accuracy in the gas-phase.[146,147] Indeed, this means that they may then be condensed on dry HA micro-crystal surfaces and their features, as adsorbed species, studied by surface FTIR techniques as done for glycine in an elegant series of experiments by Lambert's group.[148,149] Only the (001) and the (010)-RW HA surfaces have been selected to study the amino acids adsorption, because these two surfaces are the most relevant ones from a biological point of view (*vide supra*). The studied amino acids are glycine (Gly), the simplest amino acid with no lateral chain functionalities, lysine (Lys) and glutamic acid (Glu) with, respectively, basic and acidic behaviour of the their lateral chains, hence being representative of the main acid/base behaviour of the amino acid family. In order to accommodate the amino acid long side chains, a double surface unit cell for the HA models has been adopted for the calculations compared to that adopted to model the free surfaces (*vide supra*). Further results for a more extended set of amino acids will be reported in a forthcoming paper.[150]

E1 Adsorption of glycine

A detailed study of Gly adsorption has already been reported, in which an exhaustive search for possible adsorption modes was carefully exploited (see ref. 151 for further details). For the sake of brevity, only the cases of the most stable adducts are reported here. The B3LYP-D optimized structure for the (001) HA surface is shown in Fig. 13.

In this case, Gly prefers to interact with the surface in its zwitterionic state, with the COO^- group interacting electrostatically with two different Ca ions and the NH_3^+ group making H-bonds with the oxygen surface atoms. Differently, on the (010)-RW HA surface, Gly adsorbs as an anion as a consequence of a spontaneous proton transfer towards the surface (see Fig. 13), the resulting adsorbate being tightly bound through a Gly^-/HA^+ ion pair. It is reassuring that the same structures were also found recently by de Leeuw and coworkers using the PBE functional and the SIESTA code.[45] The spontaneous deprotonation of Gly on the already reacted (010)-RW HA surface highlights the strong basic character of this surface, despite having already been reacted with H_2O. The high reactive behaviour of the (010)-RW surface is indicated by the computed adsorption energies which are higher than those computed for the (001) one (see Table 4).

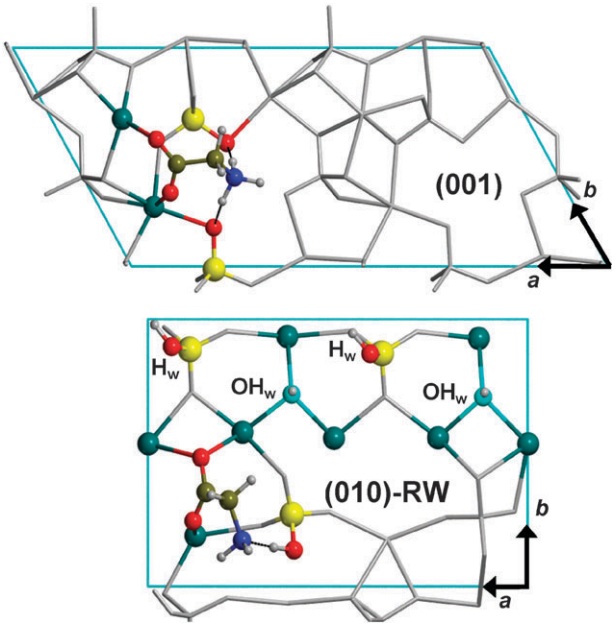

Fig. 13 HA (001) and (010)-RW unit cell with the most stable configuration of adsorbed glycine. Colour coding: Ca (cyan), P (yellow), O (red), C (green), N (blue), H (light grey). For the (010)-RW the new functionalities resulting by the reaction with water have labelled OHw and Hw, respectively.

Table 4 Computed adsorption energies of glycine, glutamic acid and lysine on the (001) and (010)-RW HA surfaces. B3LYP-D refers to re-parameterized Grimme's data set.[101] Data in kJ mol^{-1}

Amino acid/HA surface	B3LYP	B3LYP-D
Gly/(001)	−247	−306
Gly/(010)-RW	−321	−381
Lys/(001)	−341	−432
Lys/(010)-RW	−364	−482
Glu/(001)	−383	−500
Glu/(010)-RW	−379	−474

Clearly dispersive contribution to the final interaction energy is already sizeable for glycine.

E2 Adsorption of lysine and glutamic acid

The lesson learned with the Gly/HA interactions has been exploited also for the more complex cases of lysine (Lys) and glutamic acid (Glu), thereby restricting the search for possible surface configurations. The common H_2N–CHR–COOH moiety shared by all amino acids has been set up to interact with the surface in the same way as for Gly, while allowing the specific lateral chain (R: CH_2–CH_2–COOH and CH_2–CH_2–CH_2–CH_2–NH_2 for Glu and Lys, respectively) to search for the best interaction on the HA surfaces sites. On an intuitive base, for Lys, due to its basic character, the electrostatic interactions between the N lone pair and the positive region of electrostatic potential (*vide supra*) close to the most exposed Ca ions should be dominant. Conversely for Glu, due to its acidic character, the key interaction is expected to be the balance between the protonation of the P═O surface moiety and the stabilization of the carboxylate by electrostatic interactions with the exposed Ca ions. The B3LYP-D optimized

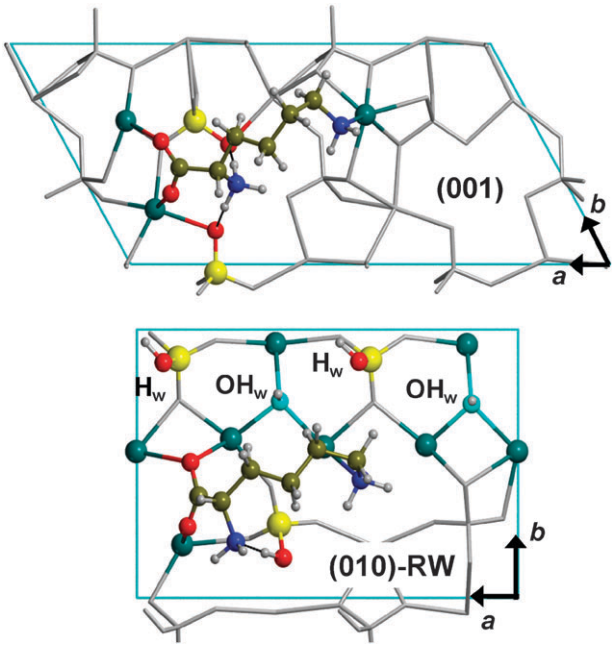

Fig. 14 Most stable configuration of lysine adsorbed on the (001) and (010)-RW HA unit cell. Colour coding: Ca (cyan), P (yellow), O (red), C (green), N (blue), H (light grey). For the (010)-RW the new functionalities resulting by the reaction with water were labelled OH_w and H_w respectively.

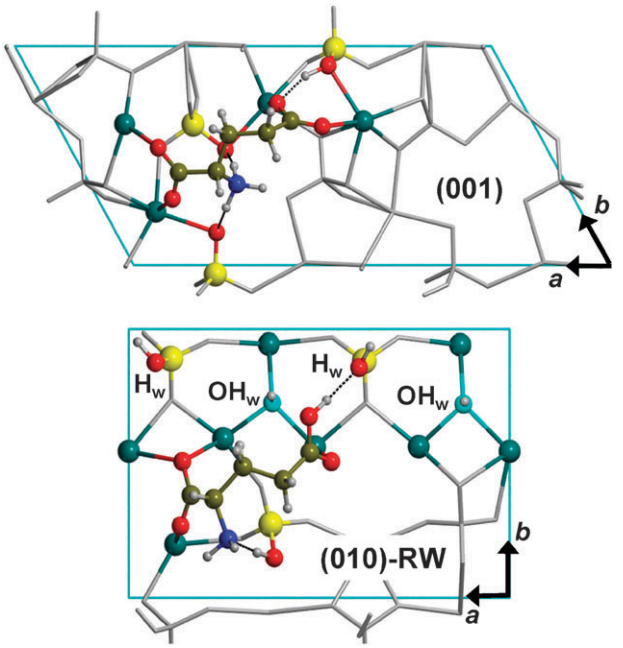

Fig. 15 Most stable configuration of glutamic acid adsorbed on (001) and (010)-RW HA unit cell. Colour coding: Ca (cyan), P (yellow), O (red), C (green), N (blue), H (light grey). For the (010)-RW the new functionalities resulting from the reaction with water were labelled OH_w and H_w respectively.

structures are shown in Fig. 14 and 15. Lys behaves very similarly on both surfaces, as the terminal N atom of the side chain is attached to the closest Ca ions (see Fig. 14). Accordingly, the naïve prediction is confirmed by quantum-mechanical calculations.

However, the fate of Glu is, surprisingly, quite dependent on the surface: on the (001) HA a spontaneous proton transfer occurs from the COOH side chain to a basic oxygen of the P═O surface moiety (see Fig. 15). The COO^- group thus formed interacts with two closest Ca ions being also engaged in a H-bond with the surface POH group resulted from the proton transfer. On the (010)-RW surface, however, the COOH moiety of the Glu side chain cannot easily release its proton toward the surface because the (010)-RW can only offer a POH group, which is a poorer H-bond acceptor than the P═O group present on the (001) surface. As Fig. 15 shows, only a moderately strong H-bond (H···O of about 1.84 Å) is formed between the COOH and the POH groups. In case the proton transfer from Glu to the HA surface occurred, a water molecule should be formed resulting in a new O═C–O–P bond.

However, looking carefully at the structure of Fig. 15 one realizes that such a process would impart definite geometric distorsion to both the Glu side chain and the surface, in order to accommodate the new bond. So, in this case, the naïve prediction is only partly fulfilled, highlighting the subtleties of the amino acid/HA interactions and the usefulness of running *ab initio* calculations to finely characterize adsorption processes on complex surfaces.

As already pointed out for Gly, the computed adsorption energies (summarized in Table 4) are sensitive to the adopted method: while B3LYP calculations which miss the dispersive contribution result in the smallest adsorption energies for all cases, the inclusion of the dispersive contribution renders the adsorption energies more negative, thus increasing the affinity to the surface. For the (001) HA surface the affinity for the amino acids follows the trend of Gly < Lys < Glu, irrespective of the adopted level of theory. This is in contrast to the trends resulting for the (010)-RW surface, in which the affinity scale is indeed the same as that for the (001) surface when B3LYP data are considered, but changes to Gly < Glu < Lys, with reverted positions for Glu and Lys compared to the (001) trend, when dispersion is included (data at B3LYP-D). This permutation can be explained as follows: B3LYP data emphasizes the electrostatic and H-bond interactions between the Glu side chain, which are stronger than for Lys, whereas dispersion favours Lys because of its longer side chain compared to Glu. This delicate balance favours Lys over Glu when competing for adsorption, at least on the (010)-RW surface.

The results obtained indicate that the interplay between electrostatic forces, H-bond interactions and dispersive contribution occurring at the HA interface stabilizes either the zwitterionic or the deprotonated forms of the amino acids, the latter being stabilized by the ion/pair interaction. These facts suggest that the HA surface does indeed behave similarly to a "solid solvent" with a basic character.

These theoretical results are in line with the results described in literature: spectroscopic and classical molecular modelling-based works suggested that, on the one hand, carboxylic and basic-containing residues are usually found in close proximity to the HA surfaces,[126,127,152–158] while on the other hand,

COO^- and NH_3^+-rich peptides are prone to be folded in an α-helix conformation upon HA adsorption, a process probably induced by the contact between the HA surface and the above residues.[157–160]

It is clear that these results are relevant to understanding the key steps by which biological structures adhere to HA-based materials (such as bones, bioactive glasses or bioceramic-based drug delivery systems).

F. Competitive adsorption at hydroxyapatite (001) surface: glycine *versus* water

In the previous section, the amino acids adsorption has been simulated considering a gas-phase/solid-surface interaction. Whereas this approach is indeed feasible by means of true experiments, as has been shown by Lambert and co-workers recently for Gly adsorbed on silica,[148,149] this model appears rather far away from the condition in which a biomaterial operates, *i.e.* in water medium. Although these results are useful to understand the intrinsic interactions, *i.e.* without external agents, between amino acids and the HA surfaces, a step forward would require the inclusion of water as a solvent. One key point in that respect is to assess whether amino acids would prefer to interact either directly with the HA surfaces or indirectly through a layer of pre-adsorbed H_2O molecules.

The main problem when dealing with solvation of an adsorbate/adsorbent system computationally is how to model the multi-layers of water molecules close to the surfaces. One possibility is to adopt classical molecular dynamics (MD), which allows considering a large box resembling the bulk water in contact with the surface. However, to obtain physically meaningful results for the amino acids/HA systems, this approach requires a properly tailored force field. While accurate force fields exist for amino acids and proteins immerse in bulk water,[161,162] and for HA (as recently developed by some of us, see ref. 130) when treated separately, there are no reliable force fields capable of properly modelling the amino acids/HA systems in presence of water, as this will require to cope not only with H-bond and dispersion but also with the much more difficult case of breaking/making bonds at the interface, as described above (*vide supra*). In view of the lack of accurate force fields, a more pragmatic solution would be to adopt *ab inito* MD (AIMD).[163] Because these calculations are based on a pseudo-potential and plane-wave approach within the DFT methodology, they are, in principle, capable of simulating all the subtleties of the system of interest. The problem is that the water slab on top of the HA surface should be thick enough to allow amino acids to be solvated by the bulk water in case they are desorbed from HA surface. Additionally, considering the interaction energy computed in the previous paragraph (for Gly 300 kJ mol^{-1}, as an average) the average time, τ, needed to wait for Gly to desorb at an even very high T = 2000 K from the surface is approximately $\tau = 10^{-13} \exp(-\Delta_a H/RT) \approx 1$ μs. This means that the MD simulation run with the usual 1 fs time step would be completely useless, needing an unattainable amount of computer resources to "see" Gly being detached from the HA surface. Obviously desorption becomes much more difficult working in physiological conditions (room temperature). Although the previous argument is, admittedly, rather rough, it gives the limits of using standard AIMD for adsorption/desorption processes characterized by relatively high interaction energies. Progress to simulate rare events as solvation/desolvation processes can indeed be handled by the potential of mean force method coupled with MD which is, however, not straightforward when the reaction coordinate is more complex than a single distance parameter.[164]

A much more straightforward approach has recently been proposed by some of us,[165] consisting in a series of static calculations in which a progressive micro-solvation of the dry interface, here exemplified by the interaction of Gly with the (001) HA surface, was carried out. The process starts from the gas-phase Gly/HA(001) structure (see Fig. 13, considering only a half unit cell), in which 5 water molecules have been added in order to mimic the first solvation shell, using as a guide for their location, structure W10 discussed above (see Fig. 11). Starting from the B3LYP optimized structure (see Fig. 16, [Gly-0w]5w/HA) one bond of those linking Gly to the HA surface has been replaced by inserting one solvent water. The water exhibiting the weakest affinity for the surface (most mobile water) was chosen as a bond replacer, and the process iterated until all the bonds directly linking Gly to the HA surface were replaced by the most mobile water. The final optimized [Gly-4w]1w/HA structure (see Fig. 16) is about 90 kJ mol^{-1} less stable than the starting one [Gly-0w]5w/HA, showing that Gly does indeed prefer a direct contact with the HA surface, the displaced water acting as a external solvation shell. Further details of the intermediate steps can be found in the original paper.[165]

Calculations can also be used to simulate the reaction in which a solvated Gly (5 water molecules as a first solvation shell) reaches a solvated (001) HA surface (using the W10 model, see Fig. 11) to give either [Gly-0w]5w/HA or [Gly-4w]1w/HA with the expulsion of five water molecules (computed as a H-bonded cluster). The reaction is strongly *exo*-energetic (ΔE_r −169 kJ mol^{-1}) for the former, indicating the high affinity of Gly for the HA surface.

The present finding is nicely in agreement with several related experimental results: (i) grazing incidence X-ray diffraction measurements carried out on the aqueous Gly-fluoroapatite (100) surface reveal that Gly contacts the surface either directly or with the co-presence of just one extra H_2O

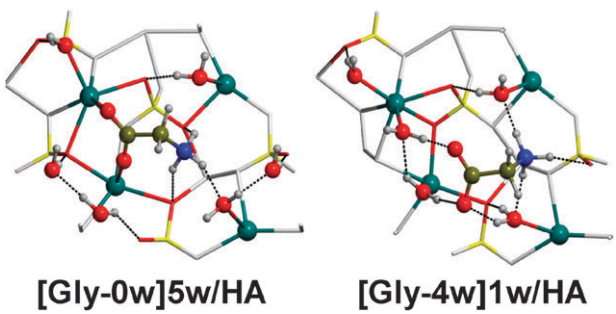

Fig. 16 HA (001) unit cell with the most stable configuration of: (left) adsorbed glycine directly bound to the surface surrounded by five co-adsorbed water molecules; (right) adsorbed glycine bridging towards the HA surface *via* pre-adsorbed water molecules.

molecule;[166] (ii) FTIR measurements on the contact between the acidic salivary proline-rich protein 1, PRP1, and HA detect the expulsion of water adsorbed on HA in favour of the formation of a direct protein–mineral interactions upon adsorption.[167]

It would be interesting to extend the present micro-solvation approach to more interesting amino acids as those already reported before. The same question asked for the case of Gly can be extended to the side chain interactions, *i.e.* whether they will be bound directly to the HA surface or *via* pre-adsorbed water. This and related questions are now in progress in our laboratory and, hopefully, this discussion will also stimulate other groups to undertake this kind of simulations.

Conclusions and perspectives

This article has highlighted the merits and limitations of studying adsorption processes occurring at the HA surfaces by means of *ab initio* methods based on well grounded quantum-mechanical techniques, *i.e.* B3LYP, Gaussian basis set and periodic boundary conditions as encoded in the CRYSTAL program.[77] Clearly, this approach has no difficulty in properly handling bond breaking/making processes or intermolecular interactions based on electrostatic and H-bond interactions. However, dispersion interactions (London forces) are unfortunately left aside by most of the current functionals (although the Minnesota 2005 hybrid *meta* functionals M05/M06 from the Thrular's group[168] improve on handling dispersion interactions). In the present case, the handy and cheap empirical *a posteriori* correction to the DFT energy as proposed by Grimme[99,100] has been adopted by means of the B3LYP-D model. This approach has been proved to be effective in predicting sublimation energies of molecular crystal[101] and adsorption energies rather accurately (*vide supra* and ref. 169). The present methodology has been applied in a consistent numerical way to predict HA bulk structural and vibrational features and the electrical features of the main HA surfaces. Furthermore, adsorption of biological relevant molecules has also been completed by exploiting the key information derived from the study of the electrostatic features of the separated entities (HA and the adsorptive). It has been proven that this approach can significantly reduce the need for exploration of the configurational space of the adsorptives on HA surfaces, a very important aspect when dealing with amino acids adsorption. The HA material and its surfaces show rather interesting physico-chemical features: the electron density and the corresponding electrostatic potential indicate a rather ionic character. However, at variance with the chemical behaviour of the ionic surface of thermally activated metal oxides, water is dissociatively adsorbed at the HA surface only in few cases and for a subset of the available surface Ca ions. This is thought to be a consequence of the covalent nature of the negative counterions of Ca^{2+} cations in HA (PO_4^{3-} groups), with respect to the basic O^{2-} moieties present in metal oxides. Furthermore, the surface becomes immediately passivated after the most active Ca ions split water, as the new OH surface functionalities stabilize the reacted HA surfaces against further water dissociation. Clearly, this behaviour has profound effects on the biological function exerted by HA, as an easy and iterated attack by water would disrupt the framework of bones and teeth. In that respect, the reactivity towards amino acid functionalities, which are tightly bound to the HA surface, can shed some light on our understanding of the interplay between protein collagen fibers and HA platelets, which is the key factor behind bones extraordinary structural and chemical features.[170]

At this point, to put this work in a future perspective, one has to assess whether this approach is suitable or not for improving our understanding of the "surface science model for biology". Clearly, the presented data indicate that only very modest steps towards the real complexity behind the "surface science model for biology" have been achieved, due to the tremendous computational cost in dealing with large systems (for instance, studying small polypeptides instead of amino acids). Fortunately, fast progress in computer architecture and computer codes development allow us to approach system sizes of definite practical interest. For instance, very recently some of us have been able to optimize at B3LYP/6-31G(d,p) level the complete 3D structure of a model of the mesoporous MCM-41 material (unit cell contains 640 atoms without symmetry) by using 128 CPUs on the massive parallel architecture at the Barcelona Supercomputing Centre (BSC).[171] Today, a system three times larger than the original MCM-41 can be handled in a local cluster using 64 CPUs, thanks to faster and cheaper processor units and further exploitation of the massive parallelism in CRYSTAL code.[172] Indeed, by adopting the developing massive parallel version of the CRYSTAL code we have recently characterized two systems of interest in the biomaterial context: (i) a large supercell of the HA(001) surface interacting with a polypeptide model; (ii) a fully reconstructed surface of 45S5 Hench's bioglass[51] (see Fig. 17). The first case was studied[173] stimulated by the nice experimental work by Capriotti *et al.*,[156] in which it was proved that HA surface can induce peptide folding due to favourable interaction between amino acid side chains and surface ions. We have chosen a HA (001) slab model envisaging 352 atoms in the unit cell and, when the polypeptide NtGly–Gly–Glu–Gly–Gly–Gly–Gly–Gly–Gly–Lys–Gly–GlyCt was adsorbed on it, a total of 462 atoms resulted in the model. Each B3LYP/6-31G(d,p) energy *plus* gradient step took about 45′ on 128 CPUs at the BSC which allows to fully optimize the whole system. The computed most stable conformation of the free model peptide resulted in a coil structure to be compared with a helix conformation when adsorbed on the HA surface. What the *ab initio* calculations revealed was that the transition between random coil towards helix induced by adsorption on HA (001) surface, can only occur when the original polypeptide is mutated in a way that it contains at least two Glu and two Lys amino acids which allow interactions with the surface ions strong enough to keep the helix in place.

As for the second case, we have recently simulated the structural and dynamical (vibrational spectrum) properties of a bulk model of 45S5 Hench's bioglass using the same approach as described in the present work.[174] The agreement with experiment was excellent, despite the rather limited unit cell size adopted for the calculations. The key point of the bioglass functionality as a biomaterial is its ability to grow a HA thin crystalline layer outside the bioactive glass particles.

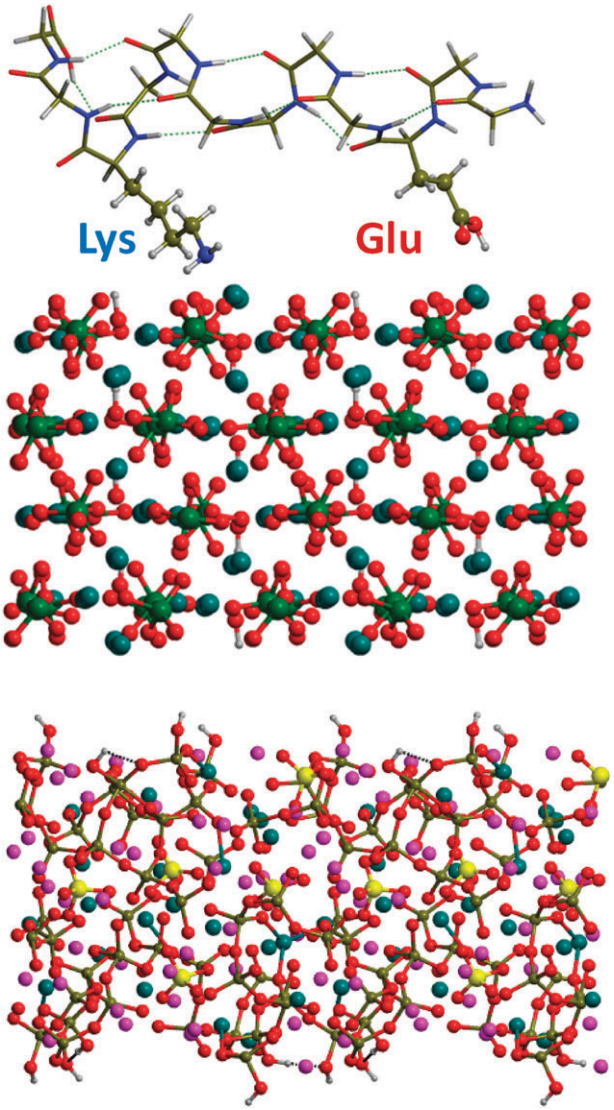

Fig. 17 Top: The NtGly–Gly–Glu–Gly–Gly–Gly–Gly–Gly–Gly–Lys–Gly–GlyCt polypeptide approaching the (001) HA surface. Bottom: PBE optimized model of a surface derived from the Hench bioglass ($Na_{40}Ca_{22}P_5Si_{41}O_{141}H_9$ composition).

This "HA skin" is then responsible for the favourable interaction between the bioactive glass and the biological environment, and it is the key factor for the integration of the implanted material within the living organism. It is then of paramount relevance to be able to model quantum-mechanically possible surfaces derived from 45S5 Hench's bioglass. It is worth remembering that Hench's bioglass is amorphous, a fact which renders the simulation of its surfaces much more involved than for the case of crystalline HA. *Ab initio* molecular dynamics data based on the CPMD code[71] have recently been reported, aiming at understanding the surface reconstruction and the reactivity with water.[175–177] In our approach MD is still too costly, so we have built a surface in which unsaturated valencies have been manually capped by silanol groups, as indeed occurs experimentally ensuring electroneutrality. To remove any large dipole moment across the slab due to the geometric cut, the structure of the starting model was initially relaxed by means of classical molecular dynamics using force fields derived by some of us to deal with silica[178] and hydroxyapatite,[130] respectively. The relaxed structure was then fully optimized at *ab initio* level using the PBE functional. The resulting slab model is shown in Fig. 17 and turned out to be almost nonpolar. As a step forward, the electrostatic potential above/below the surfaces was computed to establish the best sites for studying water and amino acid adsorption, following the methodology described previously for the HA surfaces.

Still much work remains to be done as this field is so rich in interesting points of fundamental nature to be addressed. The present work has focused on HA surfaces due to the relevance of this biomaterial. However, one should consider that the actual HA material responsible for bones and teeth features is actually carbonate hydroxyapatite of the kind of dahllite mineral,[179] in which CO_3^{2-} groups have substituted a number of the PO_4^{3-} groups in the structure, reaching 4–6% in weight of the mineral.[180,181] The modelling is here essential to understand the detailed structure of the carbonate HA, as X-ray diffraction cannot provide accurate answers due to structural disorder which characterizes these materials.[182,183] Some computational work has been carried out recently for A and B substitution in the bulk,[36,42,47,184] However, to the authors' knowledge, the modelling of carbonate hydroxy-apatite surfaces is still missing. In light of what has been discussed in this work, it would be extremely interesting to assess how CO_3^{2-} groups may affect the electrostatic properties and, consequently, the reactivity of the hydroxy-carbonate-apatite (HCA) compared with the unsubstituted HA material. Because we believe this to be an essential wedge in the definition of the "surface science model for biology" it is, at the moment, under intensive investigation in our laboratory.

Acknowledgements

Some of the largest calculations of this work have been supported by generous allowance of computer time from the Barcelona Supercomputing Centre (Projects: BCV-2008-2-0013; BCV-2008-3-0006: simulation of peptide folding induced by inorganic materials) and the CINECA computing centre. Part of this work was supported by the Italian Ministry MIUR (Project COFIN-2006, Prot. 2006032335 Interface phenomena in silica-based nanostructured biocompatible materials contacted with biological systems) and by Regione Piemonte-Italy (Project CIPE-2004, Nanotechnologies and Nanosciences Nanostructured materials biocompatible for biomedical applications). Colleagues G. Martra, L. Bertinetti, F. Chiatti (Dip. Chimica IFM, University of Torino) and C. Busco (Dip. DiSCAFF, University of Eastern Piedmont) are acknowledged for fruitful discussion and for providing the HA samples, synthesized and kindly supplied by ISTEC-CNR (Faenza, Italy), for the electrostatic potential maps and for calorimetric measurements. R. Dovesi, C. Roetti, C. Pisani, R. Orlando and B. Civalleri (Dip. Chimica IFM, University of Torino), C. M. Zicovich-Wilson (Facultad de Ciencias, Universidad Autonoma del Estado de Morelos, Mexico) and A. Pedone (Scuola Normale di Pisa, Italy) are thanked for discussion on clean surfaces, dispersion forces and force field implementations.

References

1 G. Ertl, in *Encyclopedia of Catalysis*, ed. J. T. Horvath, John Wiley & Sons, Hoboken, NJ, 2003, vol. 1, pp. 329–352.
2 R. Schlogl, in *Handbook of Heterogeneous Catalysis*, ed. G. Ertl, H. Knozinger, F. Schuth and J. Weitkamp, Wiley-VCH Verlag, Weinheim, 2nd edn, 2008, vol. 8.
3 G. A. Somorjai and J. Y. Park, *Surf. Sci.*, 2009, **603**, 1293–1300.
4 M. A. Van Hove, *Surf. Sci.*, 2009, **603**, 1301–1305.
5 E. A. Carter, *Science*, 2008, **321**, 800–803.
6 P. Huang and E. A. Carter, *Annu. Rev. Phys. Chem.*, 2008, **59**, 261.
7 C. J. Cramer and D. G. Truhlar, *Phys. Chem. Chem. Phys.*, 2009, **11**, 10757–10816.
8 J. M. Thomas and W. J. Thomas, *Principles and Practice of Heterogeneous Catalysis*, VCH, Weinheim, 1996.
9 G. Ertl, in *Les Prix Nobel*, ed. K. Grandin, Royal Swedish Academy, Stockholm, 2008, p. 116.
10 K. Honkala, A. Hellman, I. N. Remediakis, A. Logadottir, A. Carlsson, S. Dahl, C. H. Christensen and J. K. Nørskov, *Science*, 2005, **307**, 555–558.
11 D. G. Castner and B. D. Ratner, *Surf. Sci.*, 2002, **500**, 28–60.
12 S. Mizuno, H. Tochihara, Y. Matsumoto and K. Tanaka, *Surf. Sci.*, 1997, **393**, L69–L76.
13 G. H. Simon, T. Konig, M. Nilius, H. P. Rust, M. Heyde and H. J. Freund, *Phys. Rev. B: Condens. Matter Mater. Phys.*, 2008, **78**, 113401.
14 R. P. Blum, H. Niehus, C. Hucho, R. Fortrie, M. V. Ganduglia-Pirovano, J. Sauer, S. Shaikhutdinov and H. J. Freund, *Phys. Rev. Lett.*, 2007, **99**, 226103.
15 G. Pacchioni, S. Sicolo, C. Di Valentin, M. Chiesa and E. Giamello, *J. Am. Chem. Soc.*, 2008, **130**, 8690–8695.
16 V. Bolis, C. Busco and P. Ugliengo, *J. Phys. Chem. B*, 2006, **110**, 14849–14859.
17 S. Bordiga, A. Damin, F. Bonino, A. Zecchina, G. Spano, F. Rivetti, V. Bolis, C. Prestipino and C. Lamberti, *J. Phys. Chem. B*, 2002, **106**, 9892–9905.
18 V. Bolis, C. Busco, V. Aina, C. Morterra and P. Ugliengo, *J. Phys. Chem. C*, 2008, **112**, 16879–16892.
19 B. Kasemo, *Curr. Opin. Solid State Mater. Sci.*, 1998, **3**, 451.
20 *Biomaterial Science: An Introduction to Materials in Medicine*, ed. B. D. Ratner, A. S. Hoffman, F. J. Schoen and J. Lemons, Elsevier Inc., 2004.
21 D. F. Williams, J. Black and P. J. Doherty, in *Advances in Biomaterials: Biomaterial-Tissue Interfaces*, ed. P. J. Doherty, R. L. Williams, D. F. Williams and A. J. C. Lee, Elsevier Science, Amsterdam, 1992, vol. 10, pp. 525–533.
22 F. H. Jones, *Surf. Sci. Rep.*, 2001, **42**, 75–205.
23 B. Kasemo, *Surf. Sci.*, 2002, **500**, 656–677.
24 I. Van de Keere, R. Willaert, A. Hubin and J. Vereeckent, *Langmuir*, 2008, **24**, 1844–1852.
25 J. M. Kollman, L. Pandi, M. R. Sawaya, M. Riley and R. F. Doolittle, *Biochemistry*, 2009, **48**, 3877–3886.
26 R. A. Young and W. E. Brown, *Biological Mineralization and Demineralization*, Springer-Verlag, New York, 1982.
27 N. Roveri and B. Palazzo, in *Tissue, Cell and Organ Engineering*, ed. C. S. S. R. Kumar, Wiley-VCH, Weinheim, 2006, vol. 9, pp. 283–307.
28 S. V. Dorozhkin, *Materials*, 2009, **2**, 399–498.
29 S. V. Dorozhkin, *Materials*, 2009, **2**, 1975–2045.
30 L. Bertinetti, C. Drouet, C. Combes, C. Rey, A. Tampieri, S. Coluccia and G. Martra, *Langmuir*, 2009, **25**, 5647–5654.
31 M. Rouahi, E. Champion, O. Gallet, A. Jada and K. Anselme, *Colloids Surf., B*, 2006, **47**, 10–19.
32 N. Kanzaki, K. Onuma, A. T. Ito, K. Teraoka, T. Tateishi and S. Tsutsumi, *J. Phys. Chem. B*, 1998, **102**, 6471–6476.
33 K. Kandori, A. Fudo and T. Ishikawa, *Phys. Chem. Chem. Phys.*, 2000, **2**, 2015–2020.
34 K. Kandori, A. Masunari and T. Ishikawa, *Calcif. Tissue Int.*, 2005, **76**, 194–206.
35 L. Bertinetti, A. Tampieri, E. Landi, V. Bolis, C. Busco and G. Martra, *Key Eng. Mater.*, 2008, **361–363**, 87–90.
36 R. Astala and M. J. Stott, *Chem. Mater.*, 2005, **17**, 4125–4133.
37 R. Astala, L. Calderín, X. Yin and M. J. Stott, *Chem. Mater.*, 2006, **18**, 413–422.
38 R. Astala and M. J. Stott, *Phys. Rev. B: Condens. Matter Mater. Phys.*, 2008, **78**, 075427.
39 N. H. de Leeuw, *Phys. Chem. Chem. Phys.*, 2004, **6**, 1860–1866.
40 N. H. de Leeuw, *Phys. Chem. Chem. Phys.*, 2002, **4**, 3865–3871.
41 N. H. de Leeuw, *J. Phys. Chem. B*, 2004, **108**, 1809–1811.
42 S. Peroos, Z. Du and N. H. de Leeuw, *Biomaterials*, 2006, **27**, 2150–2161.
43 D. Mkhonto and N. H. de Leeuw, *J. Mater. Chem.*, 2002, **12**, 2633–2642.
44 N. H. de Leeuw and J. A. L. Rabone, *CrystEngComm*, 2007, **9**, 1178–1186.
45 N. Almora-Barrios, K. F. Austen and N. H. de Leeuw, *Langmuir*, 2009, **25**, 5018–5025.
46 M. R. T. Filgueiras, D. Mkhonto and N. H. de Leeuw, *J. Cryst. Growth*, 2006, **294**, 60–68.
47 J. A. L. Rabone and N. H. de Leeuw, *Phys. Chem. Miner.*, 2007, **34**, 495–506.
48 L. L. Hench, *Science*, 1980, **208**, 826.
49 L. L. Hench, *Biomaterials*, 1998, **19**, 1419.
50 L. L. Hench, R. J. Splinter, W. C. Allen and T. K. Greenlee, *J. Biomed. Mater. Res.*, 1971, **5**, 117–141.
51 L. L. Hench and J. Wilson, *Science*, 1984, **226**, 630.
52 L. L. Hench and J. Wilson, *An Introduction to Bioceramics*, World Scientific, Singapore, 1993.
53 L. L. Hench and J. K. West, *Life Chem. Rep.*, 1996, **13**, 187–241.
54 T. Kokubo, H. Kushitani and S. Sakka, *J. Biomed. Mater. Res.*, 1990, **24**, 721–734.
55 R. Murugan and S. Ramakrishna, *Cryst. Growth Des.*, 2005, **5**, 111.
56 I. Rehman and W. Bonfield, *J. Mater. Sci.: Mater. Med.*, 1997, **8**, 1–4.
57 H. Tsuda and J. Arends, *J. Dent. Res.*, 1994, **73**, 1703–1710.
58 R. Cuscó, F. Guitiá, S. de Aza and L. Artús, *J. Eur. Ceram. Soc.*, 1998, **18**, 1301–1305.
59 M. V. Cabanas, L. M. Rodriguez-Lorenzo and M. Vallet-Regi, *Chem. Mater.*, 2002, **14**, 3550–3555.
60 D. Rautaray, S. Mandal and M. Sastry, *Langmuir*, 2005, **21**, 5185–5191.
61 X. Qiu, Z. Hong, J. Hu, L. Chen, X. Chen and X. Jing, *Biomacromolecules*, 2005, **6**, 1193–1199.
62 L. Calderin, M. J. Stott and A. Rubio, *Phys. Rev. B: Condens. Matter Mater. Phys.*, 2003, **67**, 134106.
63 L. Calderin, D. Dunfield and M. J. Stott, *Phys. Rev. B: Condens. Matter Mater. Phys.*, 2005, **72**, 224304–224312.
64 D. Haverty, S. A. M. Tofail, K. T. Stanton and J. B. McMonagle, *Phys. Rev. B: Condens. Matter Mater. Phys.*, 2005, **71**, 094103–094109.
65 R. Dovesi, R. Orlando, B. Civalleri, C. Roetti, V. R. Saunders and C. M. Zicovich-Wilson, *Z. Kristallogr.*, 2005, **220**, 571–573.
66 R. Dovesi, B. Civalleri, R. Orlando, C. Roetti and V. R. Saunders, *Rev. Comput. Chem.*, 2005, **21**, 1–125.
67 C. Pisani, R. Dovesi and C. Roetti, in *Lecture notes in chemistry*, Springer, Berlin, Heidelberg, New York, 1988, vol. 48.
68 W. Koch and M. C. Holthausen, *A Chemist's Guide to Density Functional Theory*, Wiley-VCH, Weinheim, 2000.
69 X. Gonze, B. Amadon, P.-M. Anglade, J. M. Beuken, F. Bottin, P. Boulanger, F. Bruneval, D. Caliste, R. Caracas, M. Cote, T. Deutsch, L. Genovese, P. Ghosez, M. Giantomassi, S. Goedecker, D. R. Hamann, P. Hermet, F. Jollet, G. Jomard, S. Leroux, M. Mancini, S. Mazevet, M. J. T. Oliveira, G. Onida, Y. Pouillon, T. Rangel, G. M. Rignanese, D. Sangalli, R. Shaltaf, M. Torrent, M. J. Verstraete, G. Zerah and J. W. Zwanziger, *Comput. Phys. Commun.*, 2009, **180**, 2582–2615.
70 S. J. Clark, M. D. Segall, C. J. Pickard, P. J. Hasnip, M. J. Probert, K. Refson and M. C. Payne, *Z. Kristallogr.*, 2005, **220**, 567–570.
71 E. Hutter and M. Iannuzzi, *Z. Kristallogr.*, 2005, **220**, 549–551.
72 J. Hafner, *J. Comput. Chem.*, 2008, **29**, 2044–2078.
73 A. D. Becke, *J. Chem. Phys.*, 1993, **98**, 5648–5652.
74 C. Lee, W. Yang and R. G. Parr, *Phys. Rev.*, 1988, **B37**, 785–789.
75 F. Corà, M. Alfredsson, G. Mallia, D. S. Middlemiss, W. C. Mackrodt, R. Dovesi and R. Orlando, *Struct. Bonding*, 2004, **113**, 171–232.
76 S. F. Boys and F. Bernardi, *Mol. Phys.*, 1970, **19**, 553–566.

77 R. Dovesi, V. R. Saunders, C. Roetti, R. Orlando, C. M. Zicovich-Wilson, F. Pascale, B. Civalleri, K. Doll, N. M. Harrison, I. J. Bush, P. D'Arco and M. Llunell, *CRYSTAL06 User's Manual*, Università di Torino, Torino, 2006.
78 K. Doll, V. R. Saunders and N. M. Harrison, *Int. J. Quantum Chem.*, 2001, **82**, 1–13.
79 K. Doll, R. Orlando and R. Dovesi, *Theor. Chem. Acc.*, 2006, **115**, 354–360.
80 K. Doll, R. Dovesi and R. Orlando, *Theor. Chem. Acc.*, 2004, **112**, 394–402.
81 F. Pascale, C. M. Zicovich-Wilson, F. Lopez Gejo, B. Civalleri, R. Orlando and R. Dovesi, *J. Comput. Chem.*, 2004, **25**, 888–897.
82 C. M. Zicovich-Wilson, F. J. Torres, F. Pascale, L. Valenzano, R. Orlando and R. Dovesi, *J. Comput. Chem.*, 2008, **29**, 2268–2278.
83 S. Tosoni, F. Pascale, P. Ugliengo, R. Orlando, V. R. Saunders and R. Dovesi, *Mol. Phys.*, 2005, **103**, 2549–2558.
84 P. J. Hay and W. R. Wadt, *J. Chem. Phys.*, 1985, **82**, 284.
85 P. J. Hay and W. R. Wadt, *J. Chem. Phys.*, 1985, **82**, 299.
86 M. P. Habas and R. Dovesi, *J. Phys.: Condens. Matter*, 1998, **10**, 6897.
87 http://www.crystal.unito.it/Basis_Sets/Ptable.html, Torino, 2005.
88 P. Labeguerie, F. Pascale, M. Merawa, C. M. Zicovich-Wilson, N. Makhouki and R. Dovesi, *Eur. Phys. J. B*, 2005, **43**, 453–461.
89 F. Pascale, S. Tosoni, C. M. Zicovich-Wilson, P. Ugliengo, R. Orlando and R. Dovesi, *Chem. Phys. Lett.*, 2004, **396**, 308–315.
90 M. Prencipe, F. Pascale, C. M. Zicovich-Wilson, V. R. Saunders, R. Orlando and R. Dovesi, *Phys. Chem. Miner.*, 2004, **31**, 559–564.
91 M. Prencipe, Y. Noel, B. Civalleri, C. Roetti and R. Dovesi, *Phys. Chem. Miner.*, 2006, **33**, 519–532.
92 S. Casassa, M. Calatayud, K. Doll, C. Minot and C. Pisani, *Chem. Phys. Lett.*, 2005, **409**, 110–117.
93 P. Ugliengo, F. Pascale, M. Mérawa, P. Labéguerie, S. Tosoni and R. Dovesi, *J. Phys. Chem. B*, 2004, **108**, 13632–13637.
94 T. Bucko, J. Hafner and L. Benco, *J. Phys. Chem. B*, 2005, **109**, 7345.
95 T. Walsh, *Phys. Chem. Chem. Phys.*, 2005, **7**, 443–451.
96 X. Wu, M. C. Vargas, S. Nayak, V. Lotrich and G. Scoles, *J. Chem. Phys.*, 2001, **115**, 8748–8757.
97 X. Xu and W. Goddard III, *Proc. Natl. Acad. Sci. U. S. A.*, 2004, **101**, 2673–2677.
98 E. R. Johnson and G. A. DiLabio, *Chem. Phys. Lett.*, 2006, **419**, 333–339.
99 S. Grimme, *J. Comput. Chem.*, 2004, **25**, 1463–1473.
100 S. Grimme, *J. Comput. Chem.*, 2006, **27**, 1787–1799.
101 B. Civalleri, C. M. Zicovich-Wilson, L. Valenzano and P. Ugliengo, *CrystEngComm*, 2008, **10**, 405–410.
102 K. Doll, *Comput. Phys. Commun.*, 2001, **137**, 74–88.
103 H. B. Schlegel, *J. Comput. Chem.*, 1982, **3**, 214.
104 M. Corno, C. Busco, V. Bolis, S. Tosoni and P. Ugliengo, *Langmuir*, 2009, **25**, 2188–2198.
105 H. Takahashi, M. Yashima, M. Kakihana and M. Yoshimura, *Thermochim. Acta*, 2001, **371**, 53–56.
106 J. C. Elliott, P. E. Mackie and R. A. Young, *Science*, 1973, **180**, 1055–1057.
107 A. T. Saenger and W. F. Kuhs, *Z. Kristallogr.*, 1992, **199**, 123.
108 J. M. Hughes, M. Cameron and K. D. Crowley, *Am. Mineral.*, 1989, **74**, 870.
109 M. Corno, C. Busco, B. Civalleri and P. Ugliengo, *Phys. Chem. Chem. Phys.*, 2006, **8**, 2464–2472.
110 M. I. Kay, R. A. Young and A. S. Posner, *Nature*, 1964, **204**, 1050.
111 D. McConnell, *Apatite*, Springer-Verlag, Wien, 1973.
112 K. Sudarsanan and R. A. Young, *Acta Crystallogr., Sect. B: Struct. Crystallogr. Cryst. Chem.*, 1969, **25**, 1534.
113 W. Cao and L. L. Hench, *Ceram. Int.*, 1996, **22**, 493–507.
114 L. L. Hench, *Current Orthopaedics*, 2000, **14**, 7–15.
115 M. Vallet-Regí and J. M. González-Calbet, *Prog. Solid State Chem.*, 2004, **32**, 1–31.
116 J. Kirkham, S. J. Brookes, R. C. Shore, S. R. Wood, D. A. Smith, J. Zhang, H. Chen and C. Robinson, *Curr. Opin. Colloid Interface Sci.*, 2002, **7**, 124–132.
117 J. P. Simmer and A. G. Fincham, *Crit. Rev. Oral Biol. Med.*, 1995, **6**, 84–108.
118 C. Palache, H. Berman and C. Frondel, *The System of Mineralogy of James Dwight Dana and Edward Salisbury Dana*, John Wiley and Sons, New York, 7th edn, 1951.
119 A. Wierzbicki and H. S. Cheung, *THEOCHEM*, 2000, **529**, 73–82.
120 D. Magne, P. Pilet, P. Weiss and G. Daculsi, *Bone*, 2001, **29**, 547–552.
121 K. Sato, T. Kogure, H. Iwai and J. Tanaka, *J. Am. Ceram. Soc.*, 2002, **85**, 2142–3058.
122 K. Kandori, M. Mukai, A. Yasukawa and T. Ishikawa, *Langmuir*, 2000, **16**, 2301–2305.
123 K. Onuma, N. Kanzaki, A. Ito and T. Tateishi, *J. Phys. Chem. B*, 1998, **102**, 7833–7838.
124 N. Kanzaki, K. Onuma, G. Treboux, S. Tsutsumi and A. Ito, *J. Phys. Chem. B*, 2001, **105**, 1991–1994.
125 R. Goobes, G. Goobes, C. T. Campbell and P. S. Stayton, *Biochemistry*, 2006, **45**, 5576–5586.
126 J. R. Long, W. J. Shaw, P. S. Stayton and G. P. Drobny, *Biochemistry*, 2001, **40**, 15451–15455.
127 W. J. Shaw, J. R. Long, J. L. Dindot, A. A. Campbell, P. S. Stayton and G. P. Drobny, *J. Am. Chem. Soc.*, 2000, **122**, 1709–1716.
128 M. Corno, R. Orlando, B. Civalleri and P. Ugliengo, *Eur. J. Mineral.*, 2007, **19**, 757–767.
129 J. D. Gale, *J. Chem. Soc., Faraday Trans.*, 1997, **93**, 629.
130 A. Pedone, M. Corno, B. Civalleri, G. Malavasi, M. C. Menziani, U. Segre and P. Ugliengo, *J. Mater. Chem.*, 2007, **17**, 2061–2068.
131 A. Wander, F. Schedin, P. Steadman, A. Norris, R. McGrath, T. S. Turner, G. Thornton and N. M. Harrison, *Phys. Rev. Lett.*, 2001, **86**, 3811–3814.
132 A. Wander, I. J. Bush and N. M. Harrison, *Phys. Rev. B: Condens. Matter Mater. Phys.*, 2003, **68**, 233405–233404.
133 P. W. Tasker, *J. Phys. C: Solid State Phys.*, 1979, **12**, 4977–4984.
134 V. H. Grassian, *Surf. Sci.*, 2008, **602**, 2955–2962.
135 P. A. Thiel and T. E. Madey, *Surf. Sci. Rep.*, 1987, **7**, 211.
136 E. A. Vogler, *Adv. Colloid Interface Sci.*, 1998, **74**, 69–117.
137 E. A. Vogler, *J. Biomater. Sci., Polym. Ed.*, 1999, **10**, 1015–1045.
138 J. Israelachvili and H. Wennerstrom, *Nature*, 1996, **379**, 219–225.
139 *Water in Biomaterials Surface Science*, ed. M. Morra, John Wiley & Sons Ltd., Baffin, Lane Chichester, 2001.
140 B. Fubini, V. Bolis, M. Bailes and F. S. Stone, *Solid State Ionics*, 1989, **32–33**, 258.
141 V. Bolis, B. Fubini, L. Marchese, G. Martra and D. Costa, *J. Chem. Soc., Faraday Trans.*, 1991, **87**, 497–505.
142 V. Bolis, A. Cavenago and B. Fubini, *Langmuir*, 1997, **13**, 895–902.
143 M. Corno, F. Chiatti and P. Ugliengo, in preparation.
144 E. Artacho, D. Sanchez-Portal, P. Ordejon and A. Garcia, *Phys. Status Solidi B*, 1999, **215**, 809.
145 L. Bertinetti, A. Tampieri, E. Landi, C. Ducati, P. Midgley, S. Coluccia and G. Martra, *J. Phys. Chem. C*, 2007, **111**, 4027–4035.
146 R. Linder, M. Nispel, T. Häber and K. Kleinermanns, *Chem. Phys. Lett.*, 2005, **409**, 260–264.
147 R. Linder, K. Seefeld, A. Vavra and K. Kleinermanns, *Chem. Phys. Lett.*, 2008, **453**, 1–6.
148 M. Meng, L. Stievano and J. F. Lambert, *Langmuir*, 2004, **20**, 914–923.
149 C. Lomenech, G. Bery, D. Costa, L. Stievano and J. F. Lambert, *ChemPhysChem*, 2005, **6**, 1061–1070.
150 A. Rimola, M. Corno and P. Ugliengo, to be published.
151 A. Rimola, M. Corno, C. Zicovich-Wilson and P. Ugliengo, *J. Am. Chem. Soc.*, 2008, **130**, 16181–16183.
152 P.-H. Chen, Y.-H. Tseng, Y. Mou, Y.-L. Tsai, S.-M. Guo, S.-J. Huang, S. S.-F. Yu and J. C. C. Chan, *J. Am. Chem. Soc.*, 2008, **130**, 2862–2868.
153 J. M. Gibson, J. M. Popham, V. Raghunathan, P. S. Stayton and G. P. Drobny, *J. Am. Chem. Soc.*, 2006, **128**, 5364–5370.
154 G. Goobes, R. Goobes, W. J. Shaw, J. M. Gibson, J. R. Long, V. Raghunathan, O. Schueler-Furman, J. M. Popham, D. Baker, C. T. Campbell, P. S. Stayton and G. P. Drobny, *Magn. Reson. Chem.*, 2007, **45**, S32–S47, and references therein.

155 K. Makrodimitris, D. L. Masica, E. T. Kim and J. J. Gray, *J. Am. Chem. Soc*., 2007, **129**, 13713–13722.
156 L. A. Capriotti, T. P. Beebe and J. P. Schneider, *J. Am. Chem. Soc*., 2007, **129**, 5281–5287.
157 X. Chen, Q. Wang, J. Shen, H. Pan and T. Wu, *J. Phys. Chem. C*, 2007, **111**, 1284–1290.
158 W. J. Shaw, A. A. Campbell, M. L. Paine and M. L. Snead, *J. Biol. Chem*., 2004, **279**, 40263–40266.
159 M. L. Wallwork, J. Kirkham, J. Zhang, D. A. Smith, S. J. Brookes, R. C. Shore, S. R. Wood, O. Ryu and C. Robinson, *Langmuir*, 2001, **17**, 2508–2513.
160 H. Pan, J. Tao, X. Xu and R. Tang, *Langmuir*, 2007, **23**, 8972–8981.
161 J. W. Ponder and D. A. Case, *Adv. Protein Chem*., 2003, **66**, 27–85.
162 T. E. Cheatham III and M. A. Young, *Biopolymers*, 2000, **56**, 232–256.
163 D. Marx and J. Hutter, in *Modern Methods and Algorithms of Quantum Chemistry*, ed. J. Grotendorst, Forschungszentrum Jülich, 2000.
164 D. Trzesniak, A. E. Kunz and W. F. van Gunsteren, *ChemPhysChem*, 2007, **8**, 162–169.
165 A. Rimola, M. Corno, C. M. Zicovich-Wilson and P. Ugliengo, *Phys. Chem. Chem. Phys*., 2009, **11**, 9005–9007.
166 A. Pareek, X. Torrelles, K. Angermund, J. Rius, U. Magdans and H. Gies, *Langmuir*, 2009, **25**, 1453–1458.
167 S. Elangovan, H. C. Margolis, F. G. Oppenheim and E. Beniash, *Langmuir*, 2007, **23**, 11200–11205.
168 Y. Zhao, N. E. Schultz and D. G. Truhlar, *J. Chem. Phys*., 2005, **123**, 161103.
169 B. Civalleri, L. Maschio, P. Ugliengo and C. M. Zicovich-Wilson, *Phys. Chem. Chem. Phys*., 2010, DOI: 10.1039/c001192d.
170 R. Vanderby and P. P. Provenzano, *J. Biomech*., 2003, **36**, 1523.
171 P. Ugliengo, M. Sodupe, F. Musso, I. J. Bush, R. Orlando and R. Dovesi, *Adv. Mater*., 2008, **20**, 4579–5.
172 M. Corno, J. Garza-Olguin, I. J. Bush, R. Orlando and R. Dovesi, in preparation.
173 A. Rimola, M. Corno and P. Ugliengo, in *SimBioMa Workshop: Challenges in Modelling the Interface between biomolecules and Inorganic Surfaces*, Mainz, 2009.
174 M. Corno, A. Pedone, R. Dovesi and P. Ugliengo, *Chem. Mater*., 2008, **20**, 5610–5621.
175 A. Tilocca, *Proc. R. Soc. London, Ser. A*, 2009, **465**, 1003–1027.
176 A. Tilocca and A. N. Cormack, *ACS Appl. Mater. Interfaces*, 2009, **1**, 1324–1333.
177 A. Tilocca and A. N. Cormack, *Langmuir*, 2010, **26**, 545–551.
178 A. Pedone, G. Malavasi, M. C. Menziani, U. Segre, F. Musso, M. Corno, B. Civalleri and P. Ugliengo, *Chem. Mater*., 2008, **20**, 2522–2531.
179 S. Weiner and H. D. Wagner, *Annu. Rev. Mater. Sci*., 1998, **28**, 271–298.
180 T. S. B. Narasaraju and D. E. Phebe, *J. Mater. Sci*., 1996, **31**, 1–21.
181 N. A. M. Barakat, K. A. Khalil, F. A. Sheikh, A. M. Omran, B. Gaihre, S. M. Khil and H. Y. Kim, *Mater. Sci. Eng., C*, 2008, **28**, 1381–1387.
182 M. E. Fleet and X. Liu, *J. Solid State Chem*., 2003, **174**, 412–417.
183 M. E. Fleet and X. Liu, *J. Solid State Chem*., 2004, **177**, 3174–3182.
184 T. Guo, S. Zhou, X. Zheng and J. Jiang, *J. Phys. Chem. A*, 2009, **113**, 7112–7123.